Spatiotemporal patterns of carbon-13 in the global surface oceans and the oceanic Suess effect

Gruber, Nicolas; Keeling, Charles D.; Bacastow, Robert B.; Guenther, Peter R.; Lueker, Timothy J.; Wahlen, Martin; Meijer, Harro A. J.; Mook, Willem G.; Stocker, Thomas F.

Published in:
Global Biogeochemical Cycles

DOI:
10.1029/1999GB900019

Publication date:
1999

GLOBAL BIOGEOCHEMICAL CYCLES, VOL. 13, NO 2, PAGES 307-335, JUNE 1999

Spatiotemporal patterns of carbon-13 in the global surface oceans and the oceanic Suess effect

Nicolas Gruber,[1] Charles D. Keeling,[2] Robert B. Bacastow,[2]
Peter R. Guenther,[2] Timothy J. Lueker,[2] Martin Wahlen,[2]
Harro A. J. Meijer,[3] Willem G. Mook,[3] and Thomas F. Stocker[4]

Abstract. A global synthesis of the $^{13}C/^{12}C$ ratio of dissolved inorganic carbon (DIC) in the surface ocean is attempted by summarizing high-precision data obtained from 1978 to 1997 in all major ocean basins. The data, mainly along transects but including three subtropical time series, are accompanied by simultaneous, precise measurements of DIC concentration and titration alkalinity. The reduced isotopic ratio, $\delta^{13}C$, in the surface ocean water is governed by a balance between biological and thermodynamic processes. These processes have strongly opposing tendencies, which result in a complex spatial pattern in $\delta^{13}C$ with relatively little variability. The most distinctive feature in the spatial distribution of $\delta^{13}C$ seen in our data is a maximum of $\delta^{13}C$ near the subantarctic front with sharply falling values to the south. We attribute this feature to a combination of biological uptake of CO_2 depleted in ^{13}C (low $\delta^{13}C$) and air-sea exchange near the front and upwelling further south of waters with low $\delta^{13}C$ resulting from the remineralization of organic matter. Additional features are maxima in $\delta^{13}C$ downstream of upwelling regions, reflecting biological uptake, and minima in the subtropical gyres caused by strongly temperature dependent thermodynamic isotopic fractionation. At the time series stations, two in the North Atlantic Ocean and one in the North Pacific, distinct seasonal cycles in $\delta^{13}C$ are observed, the Pacific data exhibiting only about half the amplitude of the Atlantic. Secular decreases in $\delta^{13}C$ caused by the invasion of isotopically light anthropogenic CO_2 into the ocean (the ^{13}C Suess effect) have been identified at these time series stations and also in data from repeated transects in the Indian Ocean and the tropical Pacific. A tentative global extrapolation of these secular decreases yields a surface oceanic ^{13}C Suess effect of approximately $-0.018‰$ yr^{-1} from 1980 to 1995. This effect is nearly the same as the ^{13}C Suess effect observed globally in the atmosphere over the same period. We attribute this response to a deceleration in the growth rate of anthropogenic CO_2 emissions after 1979, which subsequently has reduced the atmospheric ^{13}C Suess effect more than the surface ocean effect.

1. Introduction

The CO_2 emitted to the atmosphere by anthropogenic activities, such as the burning of fossil fuel and changes in land use, is strongly depleted in the rare isotope ^{13}C [*Tans*, 1981; *Andres et al.*, 1996]. This is because the plants that originally produced the fuel carbon preferentially take up the light isotope ^{12}C during photosynthetic fixation of CO_2 [*O'Leary*, 1981]. As a consequence of fossil fuel combustion, the $^{13}C/^{12}C$ ratio of atmospheric CO_2 has decreased from about $-6.3‰$ in preindustrial times [*Friedli et al.*, 1986; *Francey et al.*, 1998] to about $-7.8‰$ recently [*Keeling et al.*, 1995]. In response, the $^{13}C/^{12}C$ ratios of inorganic carbon dissolved in sea water and that of organic carbon in the terrestrial biosphere presumably have also decreased since preindustrial times, although to a lesser extent [*Keeling*, 1979].

The reduction of the $^{13}C/^{12}C$ ratio in a reservoir caused by the addition of isotopically light CO_2 from

[1]Atmospheric and Oceanic Sciences Program, Princeton University, Princeton, New Jersey.
[2]Scripps Institution of Oceanography, University of California, La Jolla.
[3]Centrum voor Isotopen Onderzoek, University of Groningen, Netherlands.
[4]Climate and Environmental Physics, Physics Institute, University of Bern, Bern, Switzerland.

Paper number 1999GB900019.
0886-6236/99/1999GB900019$12.00

fossil fuel combustion is often referred to as the ^{13}C Suess effect [*Keeling*, 1979]. Observations of the ^{13}C Suess effect in the atmosphere, oceans, and terrestrial biosphere have recently received much attention because these observations constrain estimates of the redistribution of the emitted anthropogenic CO_2 within the global carbon system, most importantly the uptake of anthropogenic CO_2 by the oceans [*Quay et al.*, 1992; *Tans et al.*, 1993; *Heimann and Maier-Reimer*, 1996; *Bacastow et al.*, 1996; *Joos and Bruno*, 1998]. All of the various approaches adopted by these investigators require knowledge of the distribution of the $^{13}C/^{12}C$ ratio of dissolved inorganic carbon in the oceans.

Understanding the distribution of the $^{13}C/^{12}C$ ratio in the surface ocean is also of importance for paleoceanography because this ratio is one of the few chemical signals from past oceanic conditions that is reliably recorded by foraminifera and preserved in sediment records [*Duplessy et al.*, 1984; *Curry et al.*, 1988]. Distributions of $^{13}C/^{12}C$, inferred for the past ocean, have been used to reconstruct water mass distributions and are often regarded as a proxy for nutrient concentrations [*Charles et al.*, 1993]. This is because biological processes tend to affect $\delta^{13}C$ and nutrient concentrations proportionally. However, abiotic processes attending air-sea exchange also considerably influence the oceanic distribution of $^{13}C/^{12}C$ [*Charles and Fairbanks*, 1990; *Broecker and Maier-Reimer*, 1992; *Charles et al.*, 1993; *Lynch-Stieglitz et al.*, 1995].

Therefore, from the perspective of understanding both the present and past carbon cycles of the oceans, it is highly desirable to have a clear understanding of the distribution of the $^{13}C/^{12}C$ ratio in the ocean, its temporal variability, and controlling factors. The only attempt so far to study the distribution of the $^{13}C/^{12}C$ ratio in the oceans on a global scale was made by *Kroopnick* [1985], using his measurements obtained during the Geochemical Ocean Sections Study (GEOSECS). However, imprecision of this data (about 0.1‰, [*Kroopnick*, 1980]) and uncertain corrections of up to 0.7‰ are such that small-scale structure is not reliably resolved. Nevertheless, *Kroopnick*'s [1985] database has remained the only one available on a global scale.

This new study has three parts. First we summarize

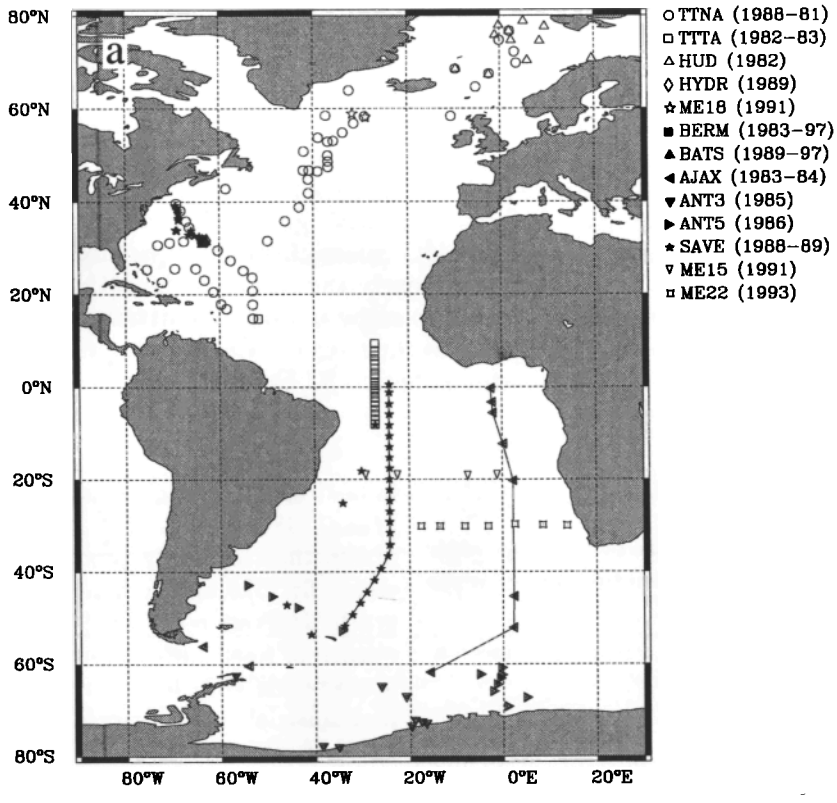

Figure 1. Station locations where the $^{13}C/^{12}C$ ratio of dissolved inorganic carbon ($\delta^{13}C$) has been measured in the upper 50 m of the ocean by the Carbon Dioxide Research Group (CDRG) of the Scripps Institution of Oceanography. (a) Station locations in the Atlantic Ocean. (b) Station locations in the Pacific Ocean. (c) Station locations in the Tropical Pacific. (d) Station locations in the Indian Ocean. Black box in Figure 1b indicates the location of the enlargement shown in Figure 1c. Pertinent information is given in Table 1 Code names and calendar years of cruises are listed for each region.

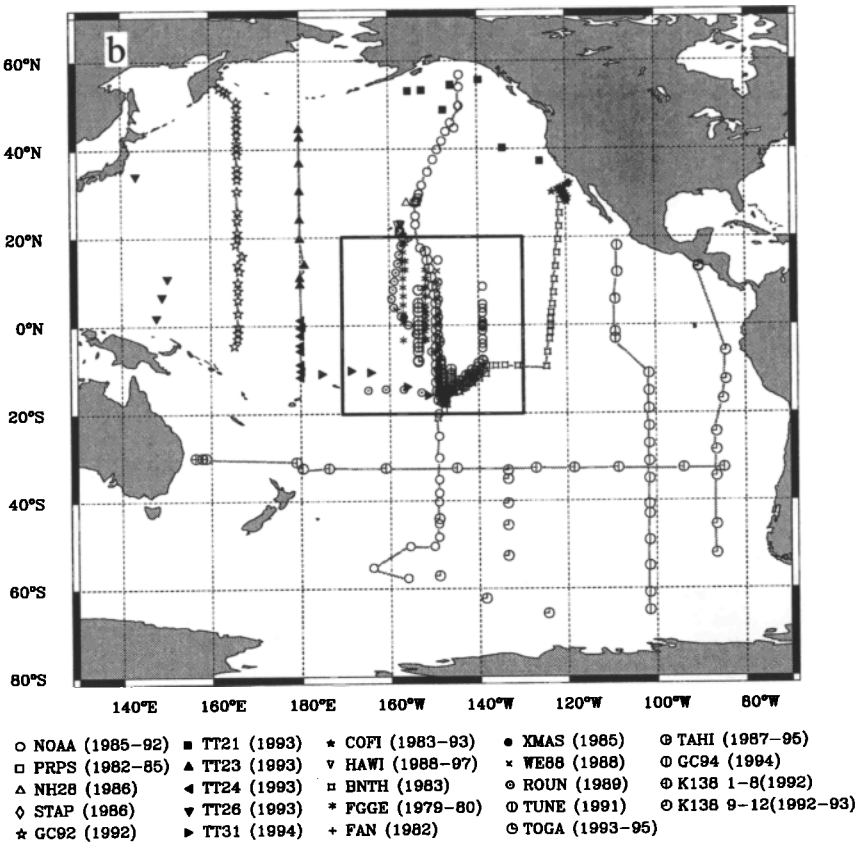

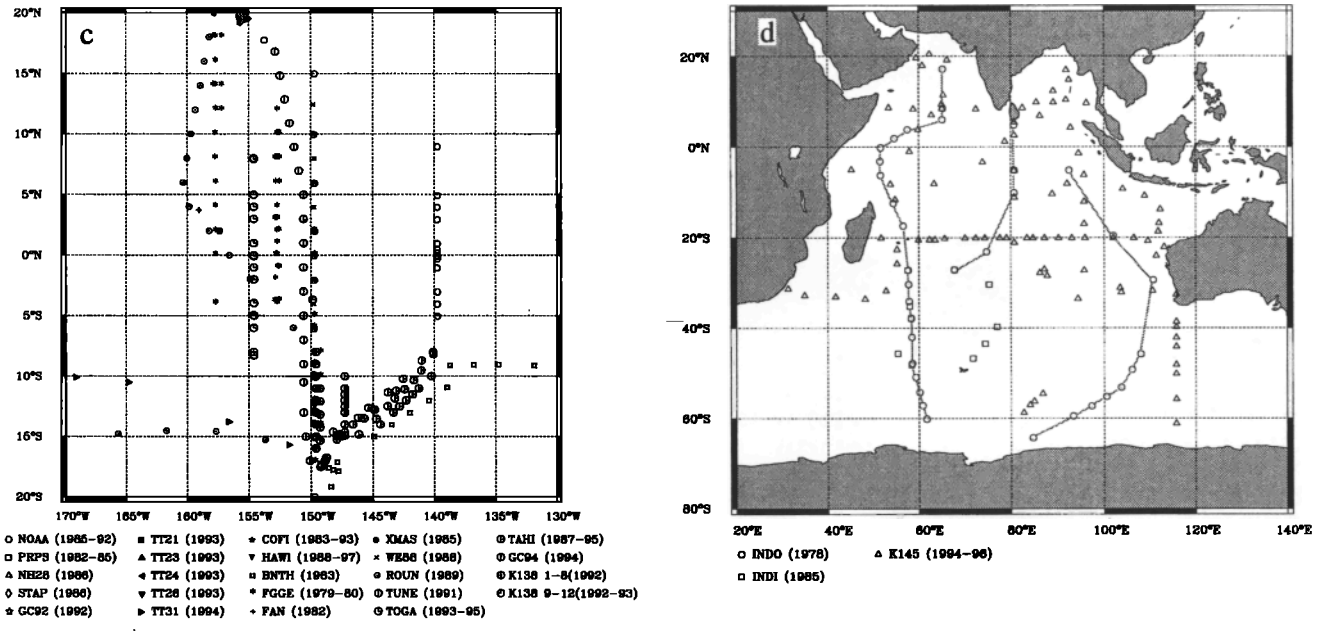

Figure 1. (continued)

measurements of the $^{13}C/^{12}C$ ratio of dissolved inorganic carbon (DIC) in the surface waters of the world oceans, obtained by the Carbon Dioxide Program of the Scripps Institution of Oceanography over a period of 19 years. We then discuss the spatiotemporal distribution of these data and factors which appear to control this distribution. Last we attempt to identify secular decreases in the $^{13}C/^{12}C$ ratio in the surface ocean.

This new data set is internally consistent, covers all major ocean basins, and allows a description of the

Table 1. Summary of Cruises and Programs

Cruise[a]	Legs	Period[b]	Region		Ship	Country[c]	Samples[d] $\delta^{13}C$	Remarks[e]
			Latitude	Longitude				
				North Atlantic				
TTNA	1-7	10/80 - 10/81	18°N-78°N	3°E-77°W	*Knorr*	USA	49	TTO N. Atl. Study
TTTA	1-3	12/82 - 2/83	8S-14°N	27°W-52°W	*Knorr*	USA	20	TTO Trop. Atl. Study
HUD		3/82	68°N-78°N	10°W-18°E	Hudson	CAN	11	wintertime cruise
SAVE	0	10/87	32°N-37°N	64°W-70°W	*Knorr*	USA	18	SAVE test cruise.
HYDR	6	5/89	31°N	63°W	*Melville*	USA	4	HYDROS
ME18	A1E	9/91	45°N-59°N	20°W-34°W	*Meteor II*	GER	2	WOCE leg A1E
BERM		9/83 - 3/97	31°N	63°W	*Weatherbird*	BER/UK	235	time series at station "S"
BATS		1/89 - 9/97	31°N	63°W	*Weatherbird*	BER/UK	55	time series at BATS
				South Atlantic				
AJAX	1,2	10/83 - 2/84	0°S-60°S	1°E-60°W	*Knorr*	USA	11	Long Lines
ANT3	3	1/85 - 2/85	62°S-77°S	17°W-58°W	*Polarstern*	GER	9	Antares III
ANT5	2-3	6/86 - 9/86	42°S-68°S	1°W-49°W	*Polarstern*	GER	9	Antares V
SAVE	1-5	10/88 - 4/89	3°N-47°S	27°W-69°W	*Knorr*	USA	30	SAVE
ME15	A9	2/91 - 3/91	23°S-19°S	9°E-30°W	*Meteor II*	GER	2	WOCE leg A9
ME22	A10	1/93	29°S-30°S	12°E-18°W	*Meteor II*	GER	7	WOCE leg A10
				North Pacific				
NOAA	85	6/85 - 7/85	23°N-57°N	144°W-154°W	*Discoverer*	USA	13	RP-9-DI-85B leg 3
PRPS		9/82	21°N-29°N	154°W-158°W	*Kila*	USA	7	PRPOOS (Climax region)
PRPS		9/85	21°N-29°N	154°W-158°W	*Melville*	USA	5	PRPOOS (Climax region)
NH28		8/86	28°N	157°W	*New Horizon*	USA	2	Hawaii
STAP		7/86 - 10/86	50°N	145°W			11	Station "P"
GC92	1,2	8/92 - 10/92	4°S-54°N	161°E-166°E	*Vickers*	USA	40	Climatic Global Change
TT21	21	5/93 - 6/93	38°N-56°N	126°W-156°E	*T. Thompson*	USA	8	WOCE leg P17N
TT23	23	6/93 - 8/93	9°N-54°N	180°W-177°E	*T. Thompson*	USA	8	WOCE leg P14
TT24	24	8/93	11°S-2°N	179°E	*T. Thompson*	USA	9	WOCE leg P14
TT26	26	10/93 - 11/93	0°N-34°N	142°E-149°E	*T. Thompson*	USA	3	WOCE leg P10
TT31	31	1/94 - 2/94	16°S-10°S	152°W-175°E	*T. Thompson*	USA	5	WOCE leg P31
COFI		3/83 - 1/93	20°N-32°N	120°W-123°W	various	USA	132	CalCOFI cruises
HAWI		10/88 - 6/97	22°N	158°W	various	USA	130	time series at HOT
				Tropical Pacific				
FGGE	1-5	4/79 - 7/79	16°S-20°N	149°W-157°W	*Gyre*	USA	31	First Global GARP Exp.
FGGE	6-15	8/79 - 5/80	16°S-20°N	149°W-157°W	*Wecoma*	USA	90	First Global GARP Exp.
FAN		9/82	3°N	159°W	*Perl*		5	Fanning Island
BNTH	7,8	4/83 - 5/83	22°S-28°N	122°W-151°W	*Melville*	USA	42	SIO Benthic cruise
XMAS		1/85	2°N	157°W	*Tasu*		5	Christmas Island
WE88		2/88 - 3/88	12°S-12°N	149°W-150°W	*Wecoma*	USA	10	W8802A cruise
ROUN	16	3/89	1°S-20°N	150°W-165°W	*Washington*	USA	18	SIO Roundabout
TUNE	1-3	6/91 - 9/91	37°S-35°N	122°W-153°W	*Washington*	USA	19	WOCE Leg P16, P17
NOAA	92	4/92 - 5/92	10°S-10°N	140°W-144°W	*Discoverer*	USA	17	EqPAC 92
TOGA		8/93 - 11/93	9°S-9°N	95°W-180°W	*Discoverer*	USA	10	DI-93-03/EPG-93DI
TOGA		8/94	8°S-5°N	155°W	*Discoverer*	USA	22	DI-94-04
TOGA		4/95	8°S-8°N	155°W	*Discoverer*	USA	16	DI-95-02
TAHI		7/83 - 10/87	8°S-16°S	140°W-150°W	various		72	Tahiti
TAHI		3/88	8°S-16°S	140°W-150°W	*Wecoma*	USA	28	Tahiti
TAHI		5/95	8°S-16°S	140°W-150°W	*Melville*	USA	9	SIO Westward 12

Table 1. (continued)

Cruise[a]	Legs	Period[b]	Region		Ship	Country[c]	Samples[d] $\delta^{13}C$	Remarks[e]
			Latitude	Longitude				
				South Pacific				
NOAA	84	2/84 - 3/84	54°S-17°N	149W-154W	*Discoverer*	USA	23	RO4-DI-84-3
K138	3-5	5/92 - 7/92	33°S-30°S	155°E-96°W	*Knorr*	USA	10	WOCE legs P6E,P6C,P6W
K138	9-10	10/92 - 12/92	65°S-33°S	126°W-150°W	*Knorr*	USA	9	WOCE legs P16S,P17S
K138	12	3/93 - 4/93	52°S-13°N	88°W-91°W	*Knorr*	USA	10	WOCE leg P19
GC94		2/94 - 4/94	65°S-18°N	111°W-103°W	*Discoverer*	USA	18	Climatic Global Change
				Indian Ocean				
~~INDO~~	4-7	1/78 - 4/78	64°S-8°N	52°E-109°E	*Knorr*	USA	33	GEOSECS Indian ocean
INDI	1	2/85 - 3/85	47°S-26°S	56°E-76°E	*M. Dufresne*	FR	12	INDIGO
K145	5	12/94 - 1/95	61°S-38°S	82°E-115°E	*Knorr*	USA	11	WOCE legs I18S, I19S
K145	6	1/95 - 3/95	31°S-17°N	80°E-102°E	*Knorr*	USA	12	WOCE les I19N
K145	7	3/95 - 4/95	33°S-1°N	78°E-114°E	*Knorr*	USA	11	WOCE legs I18N,I15E
K145	8	4/95 - 5/95	22°S - 20°S	51°E-112°E	*Knorr*	USA	17	WOCE leg I3
K145	9	6/95 - 7/95	34°S-22°S	30°E-54°E	*Knorr*	USA	7	WOCE legs I5W, I7C
K145	10	7/95 - 8/95	11°S-21°N	53°E-65°E	*Knorr*	USA	9	WOCE leg I7N
K145	11-12	8/95 - 10/95	6°N-20°N	52°E-96°E	*Knorr*	USA	10	WOCE leg I1
K145	13	11/95	24°S-10°S	108°E-112°E	*Knorr*	USA	5	WOCE leg I10
K145	14-15	12/95 - 1/96	10°S-3°S	44°E-103°E	*Knorr*	USA	6	WOCE leg I2E

[a]Cruise/program descriptor of the Carbon Dioxide Research Group.
[b]Dates are given as month/year.
[c]USA, United States of America; CAN, Canada; BER, Bermuda; UK, United Kingdom; GER, Germany; FR, France.
[d]Number indicates total number of sample pairs or single samples after quality control. Single samples constitute about 14% of the total number of samples. Quality control (see text) flagged about 5% of the $\delta^{13}C$ data.
[e]TTO, Transient Tracers in the Oceans; WOCE, World Ocean Circulation Experiment; BATS, Bermuda Atlantic Time Series Study, CalCOFI, California Cooperative Fisheries Investigation; HOT, Hawaii Ocean Time Series; GARP, Global Atmosphere Research Programme; SIO, Scripps Institution of Oceanography; GEOSECS, Geochemical Ocean Sections Study; SAVE, South Atlantic Ventilation Experiment.

spatial distribution of the $^{13}C/^{12}C$ ratio in the surface oceans in more detail than previously possible. Measurements from time series locations in the subtropical North Atlantic, the subtropical North Pacific, and the equatorial Pacific establish temporal variability of the oceanic $^{13}C/^{12}C$ ratio at these locations on both the seasonal and interannual timescales. At these stations, and in the Indian Ocean, we find indication of secular trends associated with the oceanic ^{13}C Suess effect.

The paper is organized as follows: Section 2 addresses the sampling and measurement methods employed. Sections 3-5 present the spatial distribution of the $^{13}C/^{12}C$ ratio in the surface oceans, followed by a discussion of the processes controlling the distribution. In section 6, the temporal variability is investigated at several locations. We extrapolate these trends to the global ocean and discuss the results in comparison with the atmospheric ^{13}C Suess effect over the same period.

2. Data

We report here the results of sampling surface ocean waters (at sampling depths up to 50 m) in all major ocean basins (Figures 1a-1d). In total, 1125 pairs of samples and 390 single samples have been obtained between 1978 and 1997 from a total of 58 oceanic cruises and stations as listed in Table 1. These data will be made available to the Carbon Dioxide Information and Analysis Center (CDIAC) of the World Data Center-A for Atmospheric Trace Gases, Oak Ridge National Laboratory, Oak Ridge, Tennessee. An additional 899 samples of subsurface water will be reported and discussed in another paper.

Details of the measurement procedures for DIC, titration alkalinity (Alk), and the $^{13}C/^{12}C$ ratio are given in appendix A. DIC and Alk have been normalized to a constant salinity of 35, to remove the effects of evaporation and precipitation (salinity is given on the practical salinity scale which has no units [*UNESCO*, 1981]). These normalized quantities are denoted by *s*DIC and *s*Alk, respectively. We report the $^{13}C/^{12}C$ ratio as a reduced ratio, $\delta^{13}C$ (see appendix A). All data obtained from sample pairs have been quality controlled by flagging observations wherein the difference between the analyses of two sample bottles is larger than 3 times the estimated combined error from sampling and ana-

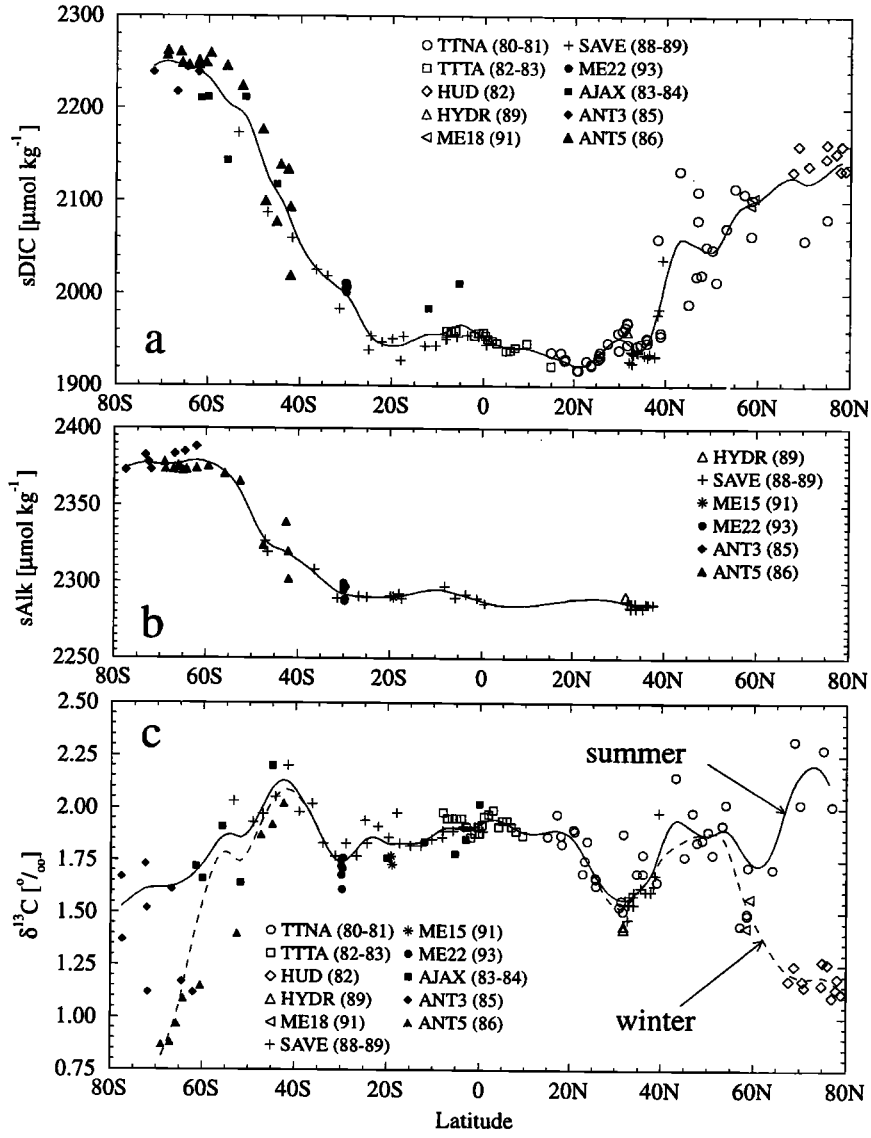

Figure 2. Meridional profiles of inorganic carbon system properties in the upper 50 m of the Atlantic Ocean: (a) normalized dissolved inorganic carbon (sDIC), (b) normalized titration alkalinity (sAlk), and (c) the reduced $^{13}C/^{12}C$ ratio of dissolved inorganic carbon ($\delta^{13}C$). Shown are the combined results of 11 cruises which span the period from 1980 to 1993. Station locations are given in Figure 1a. Smoothing spline fits have been added to emphasize the trends. For $\delta^{13}C$ (Figure 2c), two spline fits are shown to represent summer (solid curve) and winter trends (dashed curve) in the high latitudes.

lysis (2.7 μeq kg^{-1} for DIC, 4.5 μmol kg^{-1} for Alk and 0.12‰ for $\delta^{13}C$) (see appendix A for details). This has led to the removal of about 5% of the $\delta^{13}C$ data, about 9% of the DIC data, and about 8% of the Alk data. No quality control has been done for the single samples.

3. Global Surface Distributions

The results of the combined cruises and time series stations in the Atlantic, Central Pacific (from 180°-120°W), and Indian Oceans are shown as meridional profiles in Figures 2-4, respectively. The data were collected over a span of 19 years (1978 to 1997), during which atmospheric $\delta^{13}C$ decreased from approximately −7.4‰ to −7.8‰ (see *Keeling et al.* [1989, 1995], 1995 data updated with unpublished data to 1997). During the same period, atmospheric CO_2 increased from 335 to 364 parts per million by volume (ppm) [*Keeling and Whorf*, 1997]. Surface ocean DIC is expected to have followed the atmospheric CO_2 transient relatively closely [*Sarmiento et al.*, 1992; *Gruber*, 1998]. Using the global mean DIC content of surface waters (2012 μmol

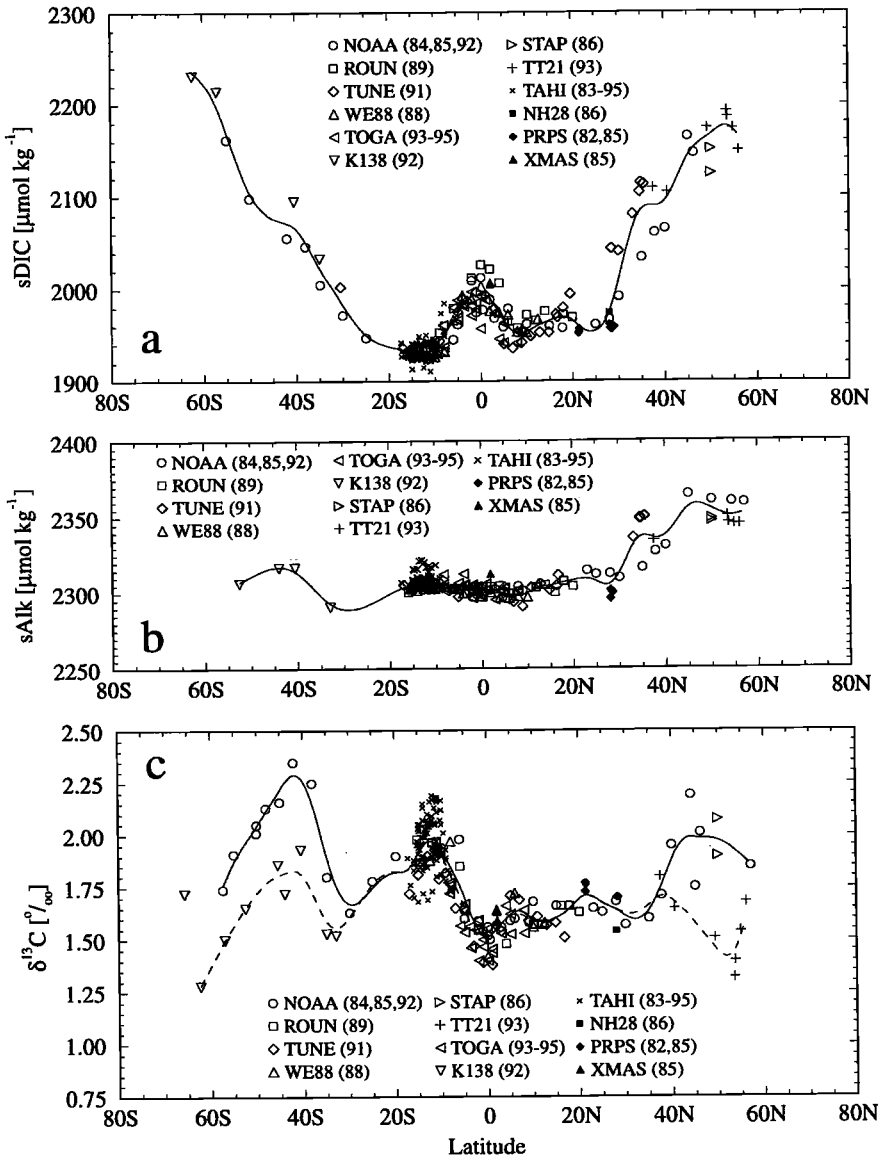

Figure 3. Same as Figure 2, except for the Central Pacific Ocean (180°-120°W). Shown are the combined results of 12 cruises which span the period from 1982 to 1995. Station locations are given in Figures 1b and 1c. For $\delta^{13}C$ (Figure 3c), two spline fits are shown to represent differing trends found in the high latitudes caused by temporal and spatial variability.

kg^{-1} [*Takahashi et al.*, 1981]) and the global surface mean Revelle factor of 10 [*Takahashi et al.*, 1980], we estimate that the average DIC concentration changed by about 17 μmol kg^{-1} over this 19 year period. Surface ocean $\delta^{13}C$ is not expected to have followed the atmospheric decrease in $\delta^{13}C$ [*Broecker and Peng*, 1993]. As will be shown in section 6, $\delta^{13}C$ in the surface waters decreased approximately 0.34‰ from 1978 to 1995, or about 0.018‰ yr^{-1}. In presenting the data, we have made no attempt to correct for these trends, and this fact must be taken into account when examining the data.

3.1. Normalized Dissolved Inorganic Carbon

Normalized DIC (*s*DIC) (Figures 2a, 3a, and 4a) exhibits a distinctly meridional pattern in all basins. The scatter of the data is relatively small compared to the large-scale meridional trend, despite the data spanning more than 19 years, all seasons, and being combined in plots across entire basins. Notable is the strong concentration difference of approximately 300 μmol kg^{-1} between low and high latitudes. This meridional trend is primarily caused by the temperature dependence of the inorganic carbon system in seawater

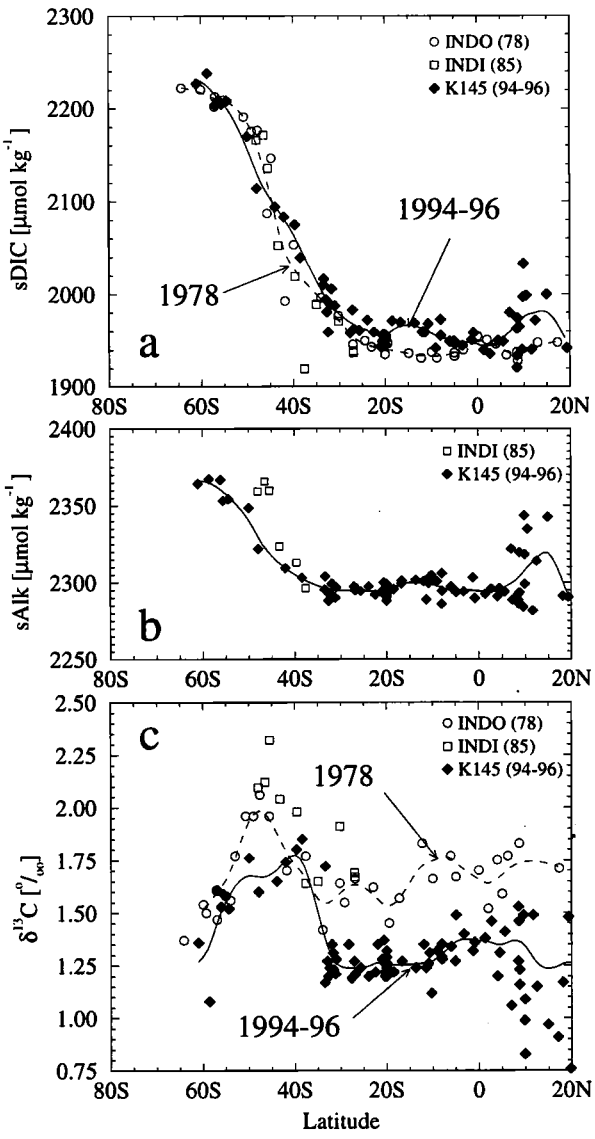

Figure 4. Same as Figure 2, except for the Indian Ocean. Shown are the combined results of 3 programs which span the period from 1978 to 1996. Station locations are given in Figure 1d. For sDIC (a) and $\delta^{13}C$ (c), two spline fits are shown to represent the change between the GEOSECS program in 1978 (solid curve) and the WOCE program in 1994-1996 (dashed curve). North of 30°S, a mean difference of 11 ± 9 μmol kg^{-1} is found for sDIC, and a mean difference of -0.34 ± 0.07‰ is found for $\delta^{13}C$. No difference could be calculated for Alk because this quantity has not been measured during GEOSECS. These long term changes reflect the addition of isotopically light anthropogenic CO_2 to the surface ocean (^{13}C Suess effect).

[*Takahashi et al.*, 1980, p. 316ff]. For typical high-latitude waters, the sDIC concentration in thermodynamic equilibrium with a reference atmospheric CO_2 concentration of 350 ppm is about 2240 μmol kg^{-1}, whereas it is about 1960 μmol kg^{-1} for low-latitude waters. Comparison of these computed values with the observations shows that to first order, sDIC is close to equilibrium with atmospheric CO_2. This is because the characteristic air-sea exchange time for CO_2 for a 50 m deep mixed layer is about 1 year [*Broecker and Peng*, 1974], short compared to the mean residence time of surface waters. Therefore large deviations from the annual mean equilibrium with the atmosphere can rarely be sustained. The meridional distribution predicted by thermodynamic processes, however, is modified by biological effects. These effects mainly influence DIC concentrations in the same direction as temperature. Net removal of DIC by photosynthesis in the low latitudes decreases sDIC, while generally, in high latitudes, upwelling of waters containing high concentrations of DIC, caused by remineralized organic matter, increases sDIC. Biological processes work in the opposite direction, however, in the tropical Pacific, where upwelling of DIC rich waters near the equator increases sDIC significantly (see Figure 3a). Elsewhere, equatorial upwelling is weaker, and its effects are less discernible.

3.2. Normalized Total Alkalinity

Normalized Alk (sAlk) exhibits considerably smaller meridional variation than sDIC (Figures 2b, 3b, and 4b). The difference for sAlk between the low latitudes and the Southern Ocean is approximately 80 μmol kg^{-1}, almost 4 times smaller than that for DIC. In the Southern Ocean (i.e., south of 50°S), the concentration of sAlk is relatively uniform at about 2380 μmol kg^{-1}; it decreases then more or less monotonically northward to values around 2300 μmol kg^{-1} at 30°S in all three ocean basins. Further north, the concentration of sAlk remains nearly constant with the exception of the North Pacific Ocean, where it increases again to around 2350 μmol kg^{-1} (Figure 3b). Alk measurements in our data set are lacking in the high-latitude North Atlantic Ocean, but *Brewer et al.* [1986] have shown that sAlk is nearly uniform over the entire North Atlantic, with a mean value of approximately 2316 μmol kg^{-1}. This value is slightly higher than the mean of the sAlk values found near 30°N but significantly lower than sAlk concentrations in the North Pacific. These almost uniform values throughout the temperate, subtropical and tropical regions appear to result from a near balance between two competing biological processes: the secretion of $CaCO_3$ shells, which reduces alkalinity, and the photosynthetic consumption of nitrate, which increases alkalinity [*Takahashi et al.*, 1980]. In the Southern Ocean, this balance is greatly disturbed by the upwelling of alkalinity-rich deep waters produced by the dissolution of calcium carbonates [*Takahashi et al.*, 1980, p. 312ff]. The contribution of this process to the high-latitude, low-latitude difference of sDIC, however, is relatively small. Even if the entire difference in sAlk between these two regions were due to the formation and dissolution of calcium carbonate, this processes would con-

tribute only about 40 μmol kg^{-1}, about 15% of the total difference in sDIC. The upwelling of alkalinity-rich deeper waters explains also the high values of sAlk in the North Pacific and its absence in the North Atlantic explains the near constancy of sAlk there, as found by *Brewer et al.* [1986].

3.3. The δ^{13}C of Dissolved Inorganic Carbon

The meridional profiles of δ^{13}C of DIC (Figures 2c, 3c, and 4c) deviate strongly from the patterns shown by sDIC and sAlk. Furthermore, between the different basins and between the different sets of measurements within the basins, the variability can be as large as the large-scale meridional variability. Most distinctive is a sharp maximum of δ^{13}C, seen in all three ocean basins at about 45°S, and roughly coinciding with the subantarctic front [*Whitworth and Nowlin*, 1987]. Near this maximum, δ^{13}C is observed to range between 1.75‰ and 2.25‰, depending on sampling time and longitude. Southward of this maximum, δ^{13}C decreases steadily. The lowest values of δ^{13}C, encountered in the Southern Ocean, vary between 0.8‰ in winter during the Antares V expedition (ANT5) and 1.5‰ in summer during the Antares III cruise (ANT3). From 45° to 30°S, δ^{13}C decreases in the Atlantic Ocean to values around 1.85‰and in the Pacific Ocean to about 1.75‰. Similarly, in the Indian Ocean north of 45°S, δ^{13}C values decrease to around 1.65‰, as observed during GEOSECS in 1978. About 17 years later during the Indian Ocean World Ocean Circulation Experiment (WOCE), values had reduced to about 1.35‰, an indication of the ^{13}C Suess effect, discussed in section 6. From 30°S to 20°N in the Atlantic and Indian Oceans, δ^{13}C shows little variability. In the Central Pacific, a second sharp maximum is found at about 15°S, with values of approximately 2.1‰ followed by a decrease to about 1.5‰ at the equator. From the equator to about 30°N, δ^{13}C is observed to be relatively constant at about 1.6‰. The western basin of the Atlantic Ocean, in contrast, shows a minimum in δ^{13}C at about 30°N. In the high latitudes of both the Atlantic and Pacific Oceans, δ^{13}C exhibits large variability with observed values between 1.1 and 2.3‰. Noteworthy is a seasonal difference observed in the Greenland-Iceland-Norwegian Seas, where the summer values sampled during the Transient Tracers in the Ocean (TTO) North Atlantic Study (NAS) (or TTNA) in 1981 were around 2.2‰, whereas during a wintertime *Hudson* cruise (HUD) half a year later, in 1982, values were near 1.1‰.

What controls the distribution of δ^{13}C in the surface ocean? This question will be addressed in section 4.

4. Processes Controlling δ^{13}C of DIC

Three main processes have to be considered in understanding the variability of surface ocean δ^{13}C. First is the combined biological processes of photosynthesis, respiration, and remineralization (soft-tissue pump); second is the formation of calcium carbonate shells and their later dissolution (carbonate pump); and third is the thermodynamic processes. The influence of each of these processes will now be summarized, largely on the basis of descriptions presented by *Broecker and Maier-Reimer* [1992] and *Lynch-Stieglitz et al.* [1995].

4.1. Biological Controls

During photosynthesis, the lighter isotope of carbon, ^{12}C, is preferentially taken up relative to the heavier isotope, ^{13}C, resulting in lower δ^{13}C values for the organic carbon in phytoplankton relative to in situ water. Typical values of δ^{13}C of marine organic matter range from −20‰ in the low latitudes and mid latitudes to −30‰ in the Southern Ocean [*Rau et al.*, 1989; *Freeman and Hayes*, 1992; *Goericke and Fry*, 1994]. A fraction of the isotopically light organic material is subsequently removed to the deeper ocean and remineralized. Biological production therefore raises the δ^{13}C of DIC in the surface waters, while upwelling of subsurface water brings with it DIC from remineralized organic matter that lowers surface δ^{13}C. In sharp contrast, only a small fractionation in ^{13}C occurs during the formation of calcium carbonate shells [*Zhang et al.*, 1995; *Spero et al.*, 1997].

4.2. Thermodynamic Controls

Kinetic fractionation of the isotopes of CO_2 occurs during transfer across the air-sea boundary layer [*Siegenthaler and Münnich*, 1981; *Zhang et al.*, 1995]. The one-way ^{13}C/^{12}C fractionation factor for transfer from atmosphere to ocean is near unity, differing from it by only about −2‰. The one-way factor for ocean to atmosphere, however, differs from unity by about −10‰, strongly dependent on temperature. Equilibrium fractionation is the ratio of the one-way factors and results in ^{13}C/^{12}C depletion in the atmosphere of about −8‰ relative to the ocean.

The temperature variation of oceanic δ^{13}C in thermodynamic equilibrium with atmospheric δ^{13}C is about −0.1‰ K^{-1} [*Mook*, 1986]. Approach to this equilibrium therefore tends to make the δ^{13}C values for cold surface waters higher than those for warm surface waters. If the surface ocean were in complete isotopic equilibrium with atmospheric δ^{13}C, the 30°C range in ocean temperatures would cause approximately a 3‰ range in oceanic δ^{13}C. However, surface δ^{13}C is almost never close to isotopic equilibrium with the atmosphere [*Broecker and Peng*, 1982] because the residence time of surface waters (the order of a few years or less) is everywhere shorter than the time (the order of 10 years) needed to equilibrate ^{13}C between the atmosphere and the oceanic mixed layer [*Broecker and Peng*, 1974; *Lynch-Stieglitz et al.*, 1995]. This latter time is 10

times longer than for the sum $^{12}C + ^{13}C$ (stable carbon) [*Broecker and Peng*, 1974]. This is because ^{13}C has to achieve isotopic equilibrium with all species of the inorganic carbon system, CO_2, H_2CO_3, HCO_3^-, and CO_3^{2-}, whereas the rate of exchange of $^{12}C + ^{13}C$ is inreased by the buffer reaction of CO_2 with CO_3^{2-} and therefore can forego the direct reaction with HCO_3^-. Since CO_2, H_2CO_3, and CO_3^{2-} constitute only about 10% of the total DIC pool, the characteristic timescale for $^{12}C + ^{13}C$ to reach equilibrium is hence about 10 times shorter (see also modeling experiments described by *Lynch-Stieglitz et al.* [1995]).

Bulk transfer of CO_2 across the air-sea inferface will also alter surface ocean $\delta^{13}C$ because gaseous CO_2 is strongly depleted in ^{13}C relative to DIC. In areas with a net uptake of atmospheric CO_2, DIC will become depleted in ^{13}C, whereas DIC will become enriched in areas of net CO_2 evasion. *Lynch-Stieglitz et al.* [1995] have estimated that this kinetic effect has the potential to induce a range of about 0.6‰ in $\delta^{13}C$ of surface seawater.

4.3. Separation Between Biological and Thermodynamic Effects

We attempt to separate biological effects on $\delta^{13}C$ of DIC from thermodynamic effects by use of a concept analogous to that employed by *Gruber et al.* [1996] for their derivation of the quasi-conservative tracer, C^*. Our separation builds on previous methods [*Charles and Fairbanks*, 1990; *Broecker and Maier-Reimer*, 1992; *Charles et al.*, 1993; *Lynch-Stieglitz et al.*, 1995] but with fewer approximations. Only a semi-quantitative description is given here. A more complete derivation is presented in appendix B.

One can eliminate the contribution of the soft-tissue pump to the distribution of $\delta^{13}C$ by using phosphate, PO_4, as an indicator of this pump, to the extent that a constant atomic ratio, $r_{C:P}$, prevails between carbon and phosphorus transferred during photosynthesis, respiration, and remineralization. The contribution of the carbonate pump can be similarly eliminated using, as an indicator, Alk corrected for nitrate cycling because the formation and dissolution of calcium carbonate changes DIC proportionally to alkalinity. Applying corrections to eliminate these contributions yields two quasi-conservative oceanic tracers, C^* and $^{13}C^*$. We denote the ratio of these two tracers, expressed in δ notation, by $\delta^{13}C^*$. This quantity, to first order, reflects only the variation in $\delta^{13}C$ induced by air-sea gas exchange, including temperature dependent equilibrium fractionation; we will call it the "air-sea signature." The difference between observed $\delta^{13}C$ and calculated $\delta^{13}C^*$, which represents, correspondingly, the contribution of biological processes, we will call the "biological signature."

The advantage of studying the quantity $\delta^{13}C^*$ can be appreciated by performing the following thought experiment. A water parcel with measured quantities DIC, $\delta^{13}C$, PO_4, and Alk, is adjusted to a constant phosphate reference value, PO_4^o, by removing or adding organic carbon with a constant $r_{C:P}$ ratio and a constant $\delta^{13}C$ value, $\delta^{13}C_{org}$. Then the alkalinity is adjusted to a constant reference value, Alk^o, by forming or dissolving calcium carbonates with a constant $\delta^{13}C$ value, $\delta^{13}C_{carb}$. The alkalinity is further adjusted to a constant nitrate value to account for proton transfer during the biological reduction and oxidation of nitrate. (In practice we can instead adjust Alk to a constant phosphate value, under the assumption of a constant atomic ratio between phosphorus and nitrogen, $r_{N:P}$, transferred during photosynthesis and remineralization). The resulting adjusted values of DIC and $\delta^{13}C$ are equivalent to C^* and $\delta^{13}C^*$. The effects of these adjustments can be expressed by the following mixing equation [*Mook et al.*, 1983]:

$$\begin{aligned} C^*\,(\delta^{13}C^*) &= \mathrm{DIC}(\,\delta^{13}\mathrm{C}) - \Delta DIC_{org}\,(\delta^{13}C_{org}) \\ &\quad -\Delta DIC_{carb}\,(\delta^{13}C_{carb}), \end{aligned} \tag{1}$$

where we subtract ΔDIC_{org} and ΔDIC_{carb}, from DIC, and compute the resultant $\delta^{13}C$ of the mixture.

$$C^* = \mathrm{DIC} - \Delta DIC_{org} - \Delta DIC_{carb}, \tag{2}$$

$$\Delta DIC_{org} = r_{C:P}(PO_4 - PO_4^o), \tag{3}$$

$$\Delta DIC_{carb} = \tfrac{1}{2}\,(\mathrm{Alk} - \mathrm{Alk}^o + r_{N:P}(PO_4 - PO_4^o)). \tag{4}$$

Solving (1) for $\delta^{13}C^*$ and using equations (2)-(4) gives the definition of $\delta^{13}C^*$ equivalent to (B24) in appendix B,

$$\begin{aligned} \delta^{13}C^* = \frac{\mathrm{DIC}}{C^*}\Bigg(\delta^{13}\mathrm{C} &- \frac{r_{C:P}\delta^{13}C_{org}}{\mathrm{DIC}}\Delta PO_4 \\ &- \frac{\delta^{13}C_{carb}}{2\ \mathrm{DIC}}(\Delta\mathrm{Alk} + r_{N:P}\Delta PO_4)\Bigg). \end{aligned} \tag{5}$$

The two expressions containing $\delta^{13}C_{org}$ and $\delta^{13}C_{carb}$, on the right-hand side of (5), represent the contribution of the soft-tissue pump and the carbonate pump, respectively. Because isotopic fractionation during the formation of carbonate shells is small and the carbonate pump usually contributes far less to variations in DIC than the soft-tissue pump, the carbonate-pump term is often neglected, although not here [*Lynch-Stieglitz et al.*, 1995].

The sum of the contributions of the combined soft-tissue and carbonate pumps forms another useful tracer, $\Delta\delta^{13}C_{bio}$, evaluated by subtracting $\delta^{13}C^*$ from the observed $\delta^{13}C$,

$$\Delta\delta^{13}C_{bio} = \delta^{13}\mathrm{C} - \delta^{13}C^*. \tag{6}$$

This biological signature, $\Delta\delta^{13}C_{bio}$, is equivalent to a linear transformation of the phosphate concentration and is nearly independent of the measured $\delta^{13}C$. This is because the fractionation of the carbonate pump is small and the ratio of DIC over C^* does not deviate strongly from unity (see also appendix B).

In computing $\delta^{13}C^*$, we have adopted for $r_{C:P}$ and $r_{N:P}$ the stoichiometric ratios of 117:1 and 16:1, respectively, from *Anderson and Sarmiento* [1995]. For the $\delta^{13}C$ value of organic matter, $\delta^{13}C_{org}$, we have assumed –20‰, a value representative for all oceans north of 45°S [*Goericke and Fry*, 1994], and for $\delta^{13}C_{carb}$, we assumed a value of 2‰. The reference value Alk^o, is set for convenience in computation equal to the global average surface value of 2310 μmol kg^{-1}, on the basis of data from GEOSECS [*Takahashi et al.*, 1981]; PO_4^o is set arbitrarily to zero.

The computed values of the two tracers, $\delta^{13}C^*$ and $\Delta\delta^{13}C_{bio}$, differ from zero by constants depending on the arbitrary values chosen for the reference concentrations PO_4^o and Alk^o. We have chosen these such that $\delta^{13}C^*$ takes on values similar to surface water $\delta^{13}C$. Higher values of $\delta^{13}C^*$ in one region relative to another region for the most part indicate a stronger influence of air-sea exchange at cold temperatures, whereas smaller $\delta^{13}C^*$ values imply less $\delta^{13}C$ enrichment due to air-sea exchange. Variations in $\delta^{13}C^*$, however, also are caused by net ocean uptake or release of atmospheric CO_2. The value of $\delta^{13}C^*$ is expected to be higher in oceanic areas of net evasion and smaller in areas of net invasion [*Keir*, 1991]. Both physical and biological processes influence the location and magnitude of the invasion and evasion of atmospheric CO_2. Therefore $\delta^{13}C^*$ cannot be used to distinguish between biological and physical controls on air-sea gas exchange.

As an aid to interpretating $\delta^{13}C^*$, we have computed yet another tracer, denoted by $\delta^{13}C_{eq}$, defined as the $\delta^{13}C$ of DIC that would exist if DIC were in equilibrium with the CO_2 content and $\delta^{13}C$ of the contemporary atmosphere. In analogy to the difference in partial pressure of CO_2 between the ocean and the atmosphere, the difference between $\delta^{13}C_{eq}$ and $\delta^{13}C$ can be thought of as the driving force for isotopic equilibration by air-sea gas exchange. In computing this tracer, we have used observed values of atmospheric $\delta^{13}C$ and CO_2 concentration, oceanic Alk, temperature, and salinity, and the fractionation factors for the inorganic carbon system of *Mook* [1986]. The DIC of the sea water is assumed to change so that the oceanic CO_2 partial pressure is the same as atmospheric CO_2. To calculate the speciation of this adjusted DIC, we have employed the dissociation constants for carbonic acid of *Mehrbach et al.* [1973] and the inorganic carbon chemistry model of *Fink* [1996]. Considerable uncertainty exists with regard to the choice of the dissociation constants [*Millero*, 1995]. Our choice was based on the recent work of *Lueker* [1998], who has found the ratio of the dissociation constants for carbonic acid to agree closely with work of *Mehrbach et al.* [1973]. Global average atmospheric $\delta^{13}C$ and CO_2 at the time of sampling have been estimated from smoothing spline fits to seasonally adjusted and combined atmospheric observations at Mauna Loa, Hawaii, and the South Pole [*Keeling and Whorf*, 1997]. In the few cases where Alk data were not available, values have been estimated from the global relationship of *Gruber et al.* [1996], which is based on salinity and the quasi-conservative tracer PO ($PO = O_2 + 170\ PO_4$) [*Broecker*, 1974].

4.4. Caveats

The formulated isotopic DIC tracer, $\delta^{13}C^*$, will represent the effect of air-sea exchange on the distribution of $\delta^{13}C$ only if the assumption of constancy regarding the stoichiometric ratios, $r_{N:P}$ and $r_{C:P}$, and regarding the $\delta^{13}C_{org}$ and $\delta^{13}C_{carb}$ values, are close to correct. Most critical are the values assigned to $r_{C:P}$ and $\delta^{13}C_{org}$, because they determine the adjustments for the soft-tissue pump. While the assumption of a constant $r_{C:P}$ ratio is supported by observational analysis [*Anderson and Sarmiento*, 1995; *Peng and Broecker*, 1987; *Takahashi et al.*, 1985], the $\delta^{13}C$ value of organic matter is known to vary substantially [*Rau et al.*, 1989; *Freeman and Hayes*, 1992; *Goericke and Fry*, 1994]. Especially in the Southern Ocean, $\delta^{13}C$ of organic matter is much more negative and reaches values of around −30‰, instead of −20‰, as assumed. Therefore $\delta^{13}C^*$ will overestimate the effect of air-sea exchange in this region. Despite this limitation, $\delta^{13}C^*$ and $\Delta\delta^{13}C_{bio}$ serve as useful proxies for separating biological from thermodynamic influences on the surface distribution of $\delta^{13}C$, as long as an approximate computation suffices.

4.5. Surface Distribution of $\delta^{13}C^*$, $\Delta\delta^{13}C_{bio}$, and $\delta^{13}C_{eq}$

The three tracers discussed above, the equilibrium value, $\delta^{13}C_{eq}$, the biological signature, $\Delta\delta^{13}C_{bio}$, and the air-sea signature, $\delta^{13}C^*$, are shown in Figures 5-7 as meridional profiles in the Atlantic, Central Pacific, and Indian Oceans. With respect to $\delta^{13}C_{eq}$, the meridional profiles show that surface ocean $\delta^{13}C$ departs almost everywhere from isotopic equilibrium with the atmosphere (Figures 5a, 6a, and 7a). Waters between about 50°S and approximately 50°N are higher in $\delta^{13}C$ than they would be at equilibrium, whereas waters poleward of 50° in both hemispheres are lower. As discussed above, these large deviations from equilibrium reflect the long characteristic timescale for surface ocean $\delta^{13}C$ to approach isotopic equilibrium with the atmosphere in the face of opposing biological and thermodynamical processes and the input of fossil fuel CO_2 depleted in ^{13}C.

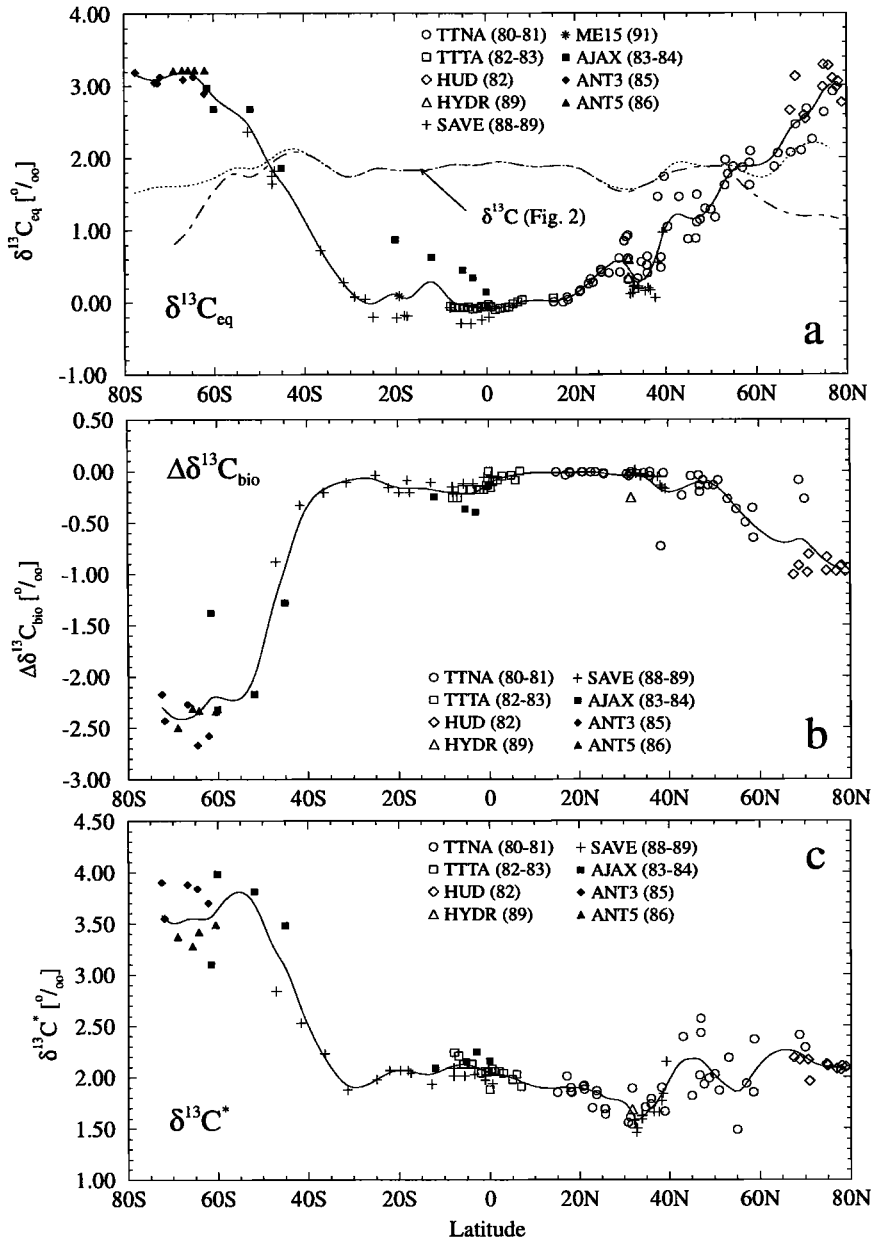

Figure 5. Meridional profiles of derived properties of $\delta^{13}C$ of dissolved inorganic carbon in the upper 50 m of the Atlantic Ocean: (a) $\delta^{13}C$ in equilibrium with the present atmospheric $\delta^{13}C$ ($\delta^{13}C_{eq}$), (b) the biological signature of $\delta^{13}C$ ($\delta^{13}C_{bio}$), and (c) the air-sea signature of $\delta^{13}C$ ($\delta^{13}C^*$). Smoothing spline fits have been added to emphasize the trends. Additionally, the spline fits through the $\delta^{13}C$ observations shown in Figure 2a have been repeated in Figure 5a. In the case of the TTNA, TTTA, HUD, and AJAX cruises, Alk has has been estimated from the global relationship of *Gruber et al.* [1996] in order to estimate $\delta^{13}C_{eq}$, $\delta^{13}C_{bio}$, and $\delta^{13}C^*$.

This is in strong contrast to DIC, which has a characteristic air-sea exchange timescale of 1 year and therefore remains relatively close to equilibrium.

With respect to $\Delta\delta^{13}C_{bio}$ and $\delta^{13}C^*$, which sum to the observed $\delta^{13}C$, both show large variations compared to $\delta^{13}C$, itself. In the upwelling regions of the tropics, in the Southern Ocean, and in the North Pacific, where phosphate is not completely removed by biological processes, $\Delta\delta^{13}C_{bio}$ attains high negative values, highlighting the large potential change of $\delta^{13}C$ that can be induced biologically. In two of these regions, the Southern Ocean south of 50°S and the North Pacific north of 40°N, $\delta^{13}C^*$ attains high positive values, indicating that these cold waters are significantly influenced

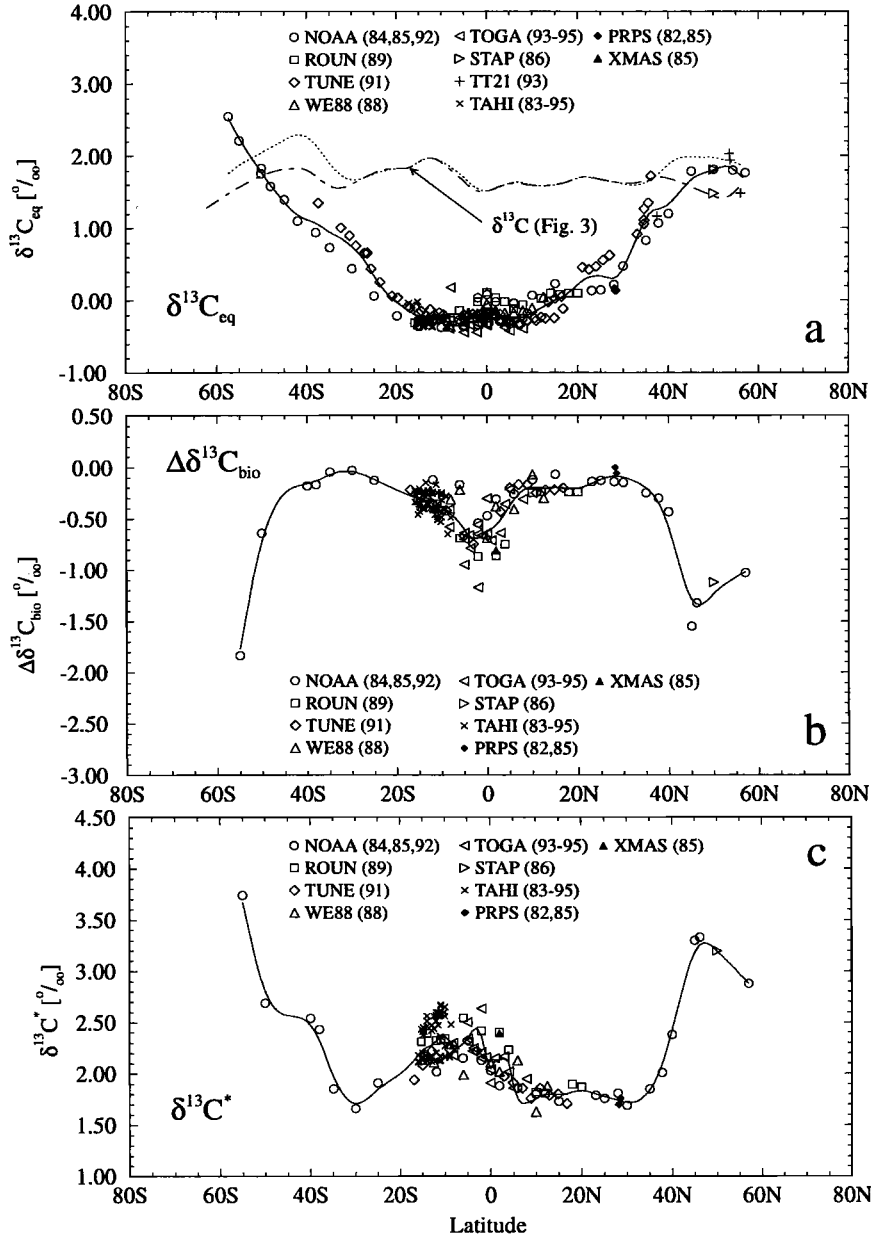

Figure 6. Same as Figure 5, but for the Central Pacific Ocean. The spline fits through the δ^{13}C observations shown in Figure 3a have been repeated in Figure 6a.

by air-sea exchange, despite their short residence time at the sea surface, 2 years or less [*Gordon*, 1988]. In the subtropics, where temperatures are relatively high and surface waters have time to approach isotopic equilibrium with the atmosphere, low values of $\delta^{13}C^*$ are found. Here $\Delta\delta^{13}C_{bio}$ is near zero, and $\delta^{13}C^*$ is therefore close to observed δ^{13}C.

Combining information contained in these three tracers, the observed variability of δ^{13}C in surface waters can now be better understood. On the global scale, the relatively small range of variability, compared to the large potential range, indicates that biological effects on δ^{13}C nearly offset thermodynamic effects [*Broecker and Maier-Reimer*, 1992]. This is well illustrated in the Central Pacific Ocean of the Southern Hemisphere (Figures 3 and 6), where upwelling near the equator brings deep waters to the surface with δ^{13}C of approximately 1.5‰, $\Delta\delta^{13}C_{bio}$ around –0.7‰ and $\delta^{13}C^*$ near 2.2‰.

These upwelled waters subsequently flow southward near the surface, forced by Ekman transport. In the process, PO_4 and isotopically light DIC are taken up during photosynthesis, and δ^{13}C increases by about

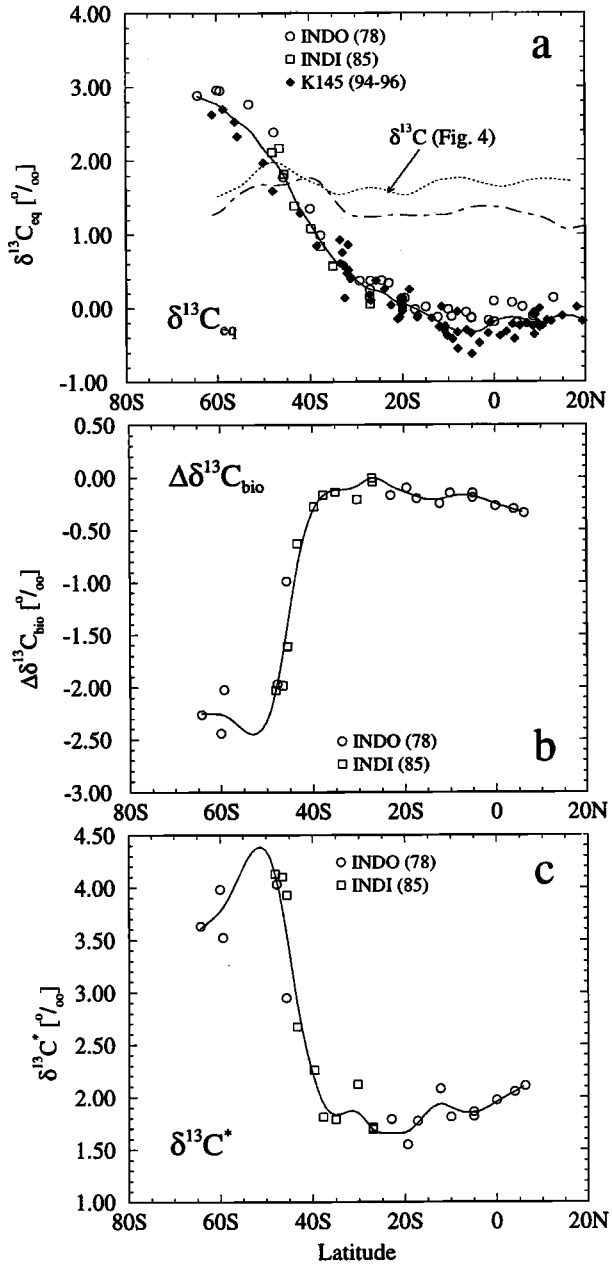

Figure 7. Same as Figure 5, but for the Indian Ocean. The spline fits through the δ^{13}C observations shown in Figure 4a have been repeated in Figure 7a. In the case of INDO, Alk has been estimated from the global relationship of *Gruber et al.* [1996] in order to calculate $\delta^{13}C_{eq}$, $\delta^{13}C_{bio}$, and $\delta^{13}C^*$.

0.5‰, to a distinct maximum at about 15°S. This increase is nearly identical to the increase in $\Delta\delta^{13}C_{bio}$, with little change in $\delta^{13}C^*$, indicating that the maximum is almost entirely a result of biological processes subsequent to upwelling. As these waters are transported further southward toward the subtropical convergence zone at about 30°S, air-sea exchange becomes the dominant process. From 15° to 30°S, biological processes (as indicated by $\Delta\delta^{13}C_{bio}$) produce an increase in δ^{13}C of only about 0.2‰, whereas air-sea exchange at these high temperatures reduces δ^{13}C by about 0.6‰ (as shown by a decrease in $\delta^{13}C^*$), resulting in the observed overall decrease of approximately 0.4‰. Air-sea exchange in these nutrient depleted regions therefore has sufficient time to mask the biological effects.

In the Atlantic and Indian Oceans, upwelling near the equator is much less pronounced than in the Pacific Ocean. In the temperate, subtropical, and tropical regions of these oceans, a balance is almost achieved between biological and thermodynamic controls of δ^{13}C, resulting in little spatial variability.

In the Southern Ocean, biological and thermodynamic controls are strongly opposed. Upwelled waters south of the subantarctic front exhibit δ^{13}C values between 1 and 1.5‰, $\Delta\delta^{13}C_{bio}$ between −2 and −2.5‰, and $\delta^{13}C^*$ between 3.5 and 4‰ (Figures 5-7). As these waters flow northward, driven by Ekman drift, net biological uptake results in a δ^{13}C increase of about 2‰ (increase in $\Delta\delta^{13}C_{bio}$). This change is largely compensated by the influence of air-sea exchange which causes a reduction of δ^{13}C of about 1.5‰ (decrease in $\delta^{13}C^*$), explaining the relatively small observed change of δ^{13}C between 60° and 45°S (Figures 2-4).

The separation of δ^{13}C into the two terms, $\Delta\delta^{13}C_{bio}$ and $\delta^{13}C^*$, permits us to explain also the large seasonal variability of δ^{13}C observed in the high-latitude North Atlantic (Figures 2 and 5). The low δ^{13}C values encountered during the winter *Hudson* cruise are a result of recent convectively mixed waters which have high absolute $\Delta\delta^{13}C_{bio}$ values (about −1.0‰). Upon stratification, biological processes remove the nutrients and isotopically light DIC, resulting in an increase of $\Delta\delta^{13}C_{bio}$ of around 1.0‰ between this cruise and the TTO NAS (TTNA) cruise of the subsequent summer. This increase is almost identical to the observed difference in δ^{13}C of about 1‰ between these two cruises, indicating little contribution of air-sea gas exchange to the seasonal variability (i.e., little change in $\delta^{13}C^*$).

Air-sea gas exchange must, however, be responsible for the relatively low $\delta^{13}C^*$ values observed in the North Atlantic (around 2.3‰) compared to the North Pacific (around 3.3‰). A fraction of the difference between these two regions can be explained by the circumstance that the North Atlantic at the same latitudes is warmer than the North Pacific. The residual difference, as discussed by *Lynch-Stieglitz et al.* [1995], is likely caused by the North Atlantic being a region of a stronger net invasion of atmospheric CO_2 compared to the North Pacific.

In summary, the spatial distribution of oceanic δ^{13}C results from a complex interaction of biological and thermodynamic controls which act largely in opposition

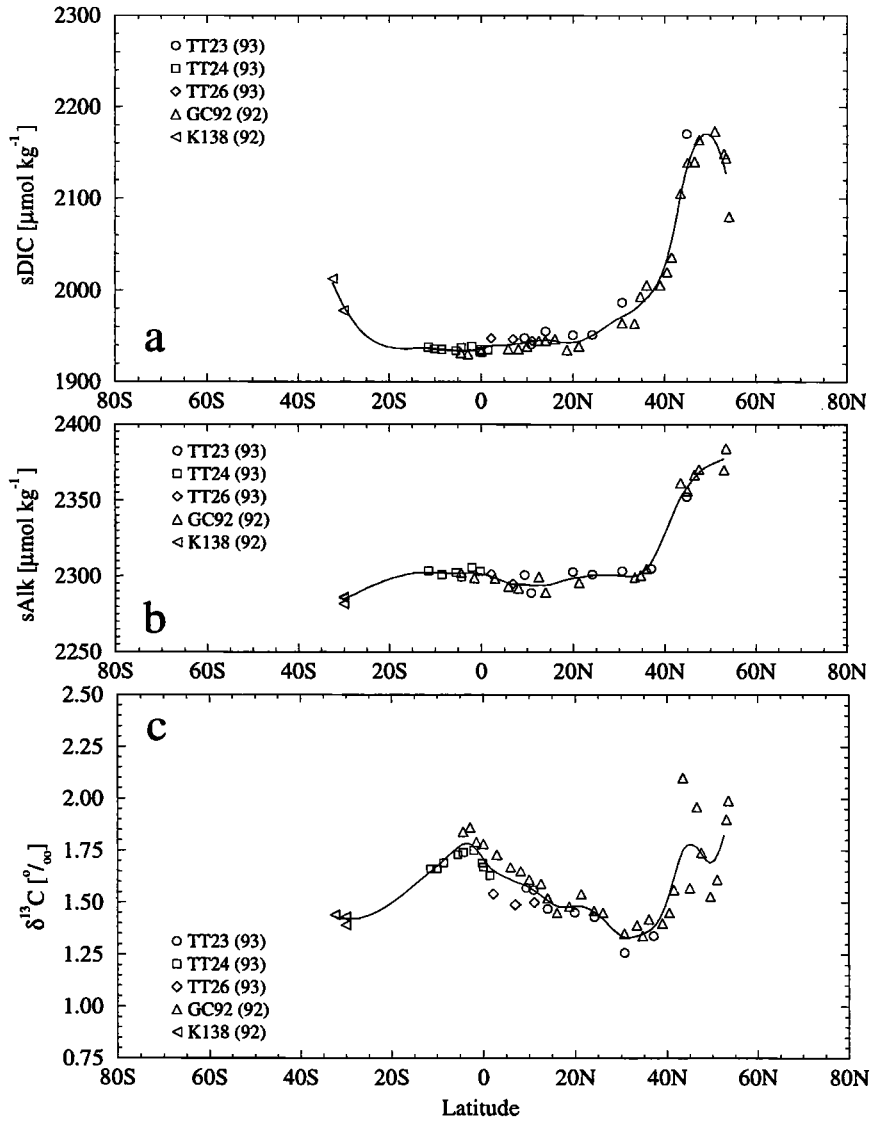

Figure 8. Meridional profiles of inorganic carbon system properties in the upper 50 m of the Western Pacific Ocean (west of 180°E): (a) normalized dissolved inorganic carbon (sDIC), (b) normalized total alkalinity (sAlk), and (c) the $^{13}C/^{12}C$ ratio of dissolved inorganic carbon ($\delta^{13}C$). Shown are the combined results of five programs which span the period from 1992 to 1993. Station locations are given in Figure 1b. Smoothing spline fits have been added to emphasize the trends.

to each other. This leads to a small spatial variability compared to the maximum potential changes that can be induced by biological or thermodynamic processes alone. The observed pattern reflects only the residual of these two processes.

5. Surface Distributions in the Pacific Ocean

The extensive spatial and temporal coverage in our data for the Pacific Ocean permits us to investigate the surface ocean distribution of $\delta^{13}C$ there in more detail than in other ocean basins. The meridional profiles of sDIC and sAlk in the western Pacific (west of 180°E, Figures 8a and 8b) show trends similar to those observed in the Central Pacific (Figure 3), except that a strong equatorial upwelling signal is lacking. Here, $\delta^{13}C$ shows a maximum near 4°S of about 1.75‰; it decreases toward the centers of the subtropical gyres at 30°N and 30°S, to values between 1.35 and 1.40‰. North of 30°N, it increases again and is more variable. This latter pattern is similar to that observed in the central Pacific. The associated patterns of $\Delta\delta^{13}C_{bio}$ and $\delta^{13}C^*$ (not shown) reveal that the maximum in $\delta^{13}C$ observed just south of the equator is mainly caused by biological processes and reflects uptake of isotopically

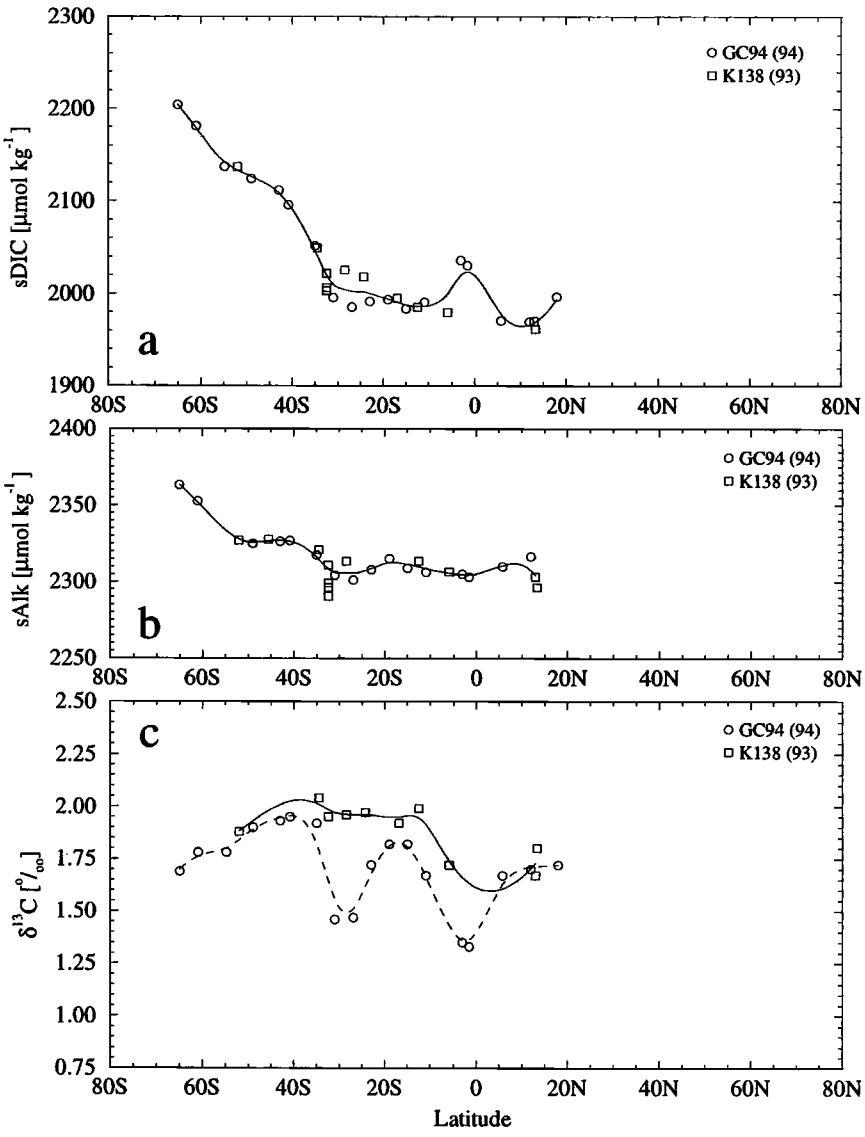

Figure 9. Same as Figure 8, except for the eastern Pacific Ocean (east of 120°W). Shown are the combined results of two cruises which span the period from 1993 to 1994. For $\delta^{13}C$ (Figure 9c), two spline fits are shown to represent the different trends exhibited by the two different cruises.

light carbon by photosynthesis, fed from PO_4 upwelling near the equator further east, a mechanism similar to that responsible for generating the maximum found at about 15°S in the Central Pacific. Then, further south in the nutrient-poor subtropic gyres of both regions, air-sea exchange drives $\delta^{13}C$ to lower values.

In the eastern Pacific (Figure 9), *s*DIC and *s*Alk show similar meridional variability to that found further west. So also does $\delta^{13}C$, as far east as the meridional profile sampled by the Climatic Global Change 1994 cruise (GC94), i.e., to about 100°W. Further east, however, the characteristic minimum of $\delta^{13}C$ found at about 30°S is completely absent on the WOCE leg P19 transect (K138). The distribution of $\delta^{13}C^*$ and $\Delta\delta^{13}C_{bio}$ (not shown) reveals that near 30°S, this difference is caused by both gas exchange and biological processes. At this latitude, the WOCE P19 cruise encounted waters lying within the transition zone between upwelling waters near Chile and subsurface nutrient-depleted waters (central water) of the east South Pacific. Upwelling of high PO_4 waters to the east of the P19 transect, with accompaning photosynthesis downstream and tempering air-sea exchange, explains the greater increase in observed $\delta^{13}C$ than that found further west.

Zonal variability at 30°S in the Pacific Ocean is revealed in more detail by also considering results of WOCE leg P6 (K138) (Figure 10). On this cruise, upwelling near the coast of Chile led to slightly elevated

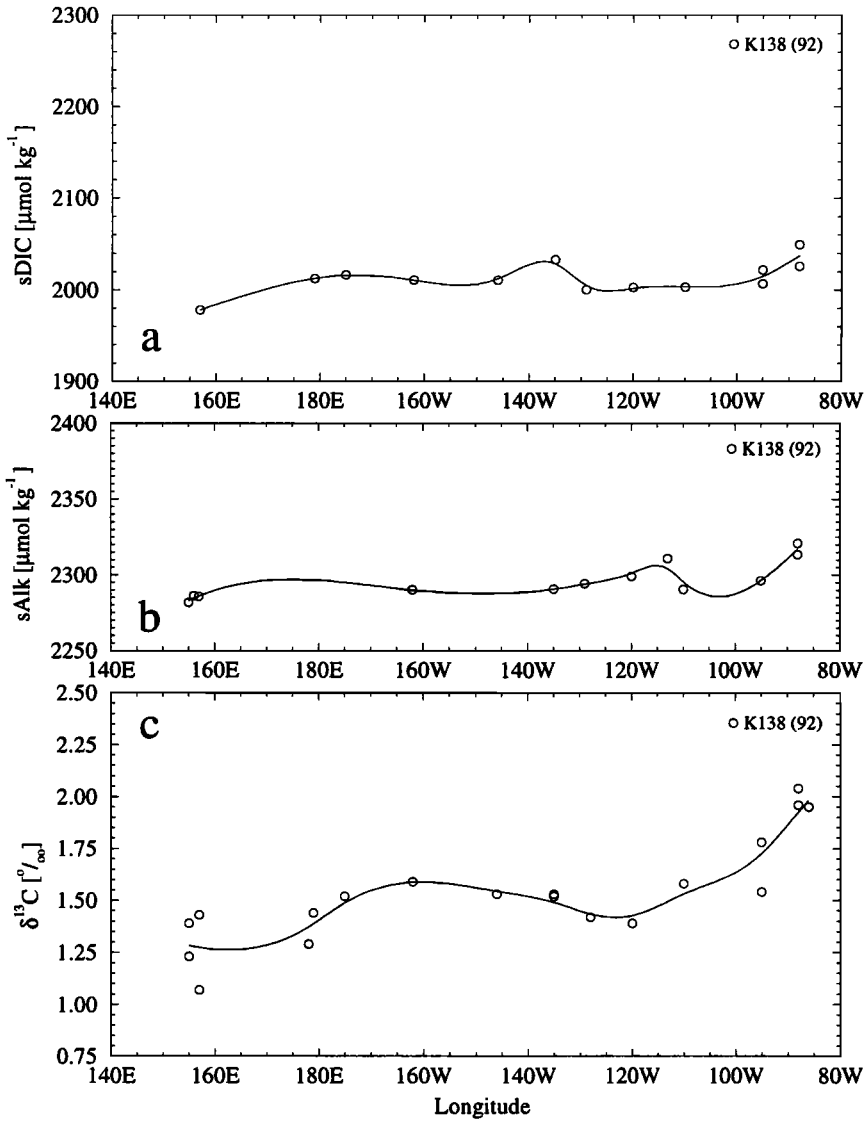

Figure 10. Same as Figure 8, but for zonal profiles of of the South Pacific Ocean along 30°S. The results shown are for the WOCE leg P6 (K138) sampled in 1992.

concentrations of sDIC and sAlk, but further west, sDIC and sAlk were remarkably uniform. In contrast, δ^{13}C decreased substantially (by about 0.5‰) from 90° to 120°W, consistent with the isotopic difference found between meridional transects GC94 and K138 (see Figure 9c). From 120° to 170°W, δ^{13}C remained relatively constant, but still further west, δ^{13}C decreased by about 0.25‰. As discussed above, we explain the large zonal trend in the eastern Pacific primarily as the result of biological processes in the east and by air-sea exchange further west.

6. Temporal Variations and the Oceanic ^{13}C Suess Effect

We now turn to describing temporal variations in three oceanic regions with repetitive sampling: the Sargasso Sea, the subtropical North Pacific, and the Central Tropical Pacific. The temporal trend indicated by a pair of transects 17 years apart in the subtropical and tropical Indian Ocean will also be described. Results up to 1991 have already been presented and discussed by *Keeling* [1993], and results for the Sargasso Sea up to 1995 have been presented by *Bacastow et al.* [1996]. We will focus on secular trends in oceanic δ^{13}C, especially the expected reduction associated with the ^{13}C Suess effect.

6.1. Time Variations Near Bermuda

Our most extensive repetitive sampling has been at Hydrostation "S" (BERM) in the northwestern Sargasso Sea, near Bermuda, where δ^{13}C, DIC, and Alk variations have been documented from observations of

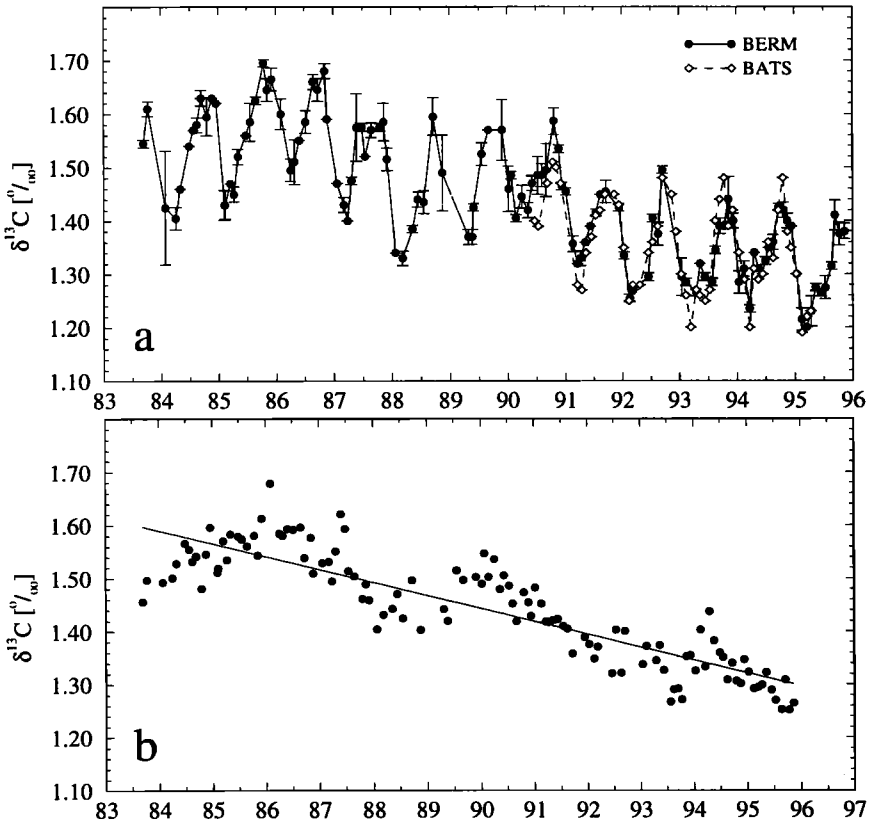

Figure 11. Time series of $\delta^{13}C$ in the northwestern Sargasso Sea near Bermuda for two locations (Hydrostation "S" (BERM) at 32°10'N, 64°30'W (solid circles); Bermuda Atlantic Time Series Study (BATS) site at 31°50'N, 64°10'W (open diamonds)). (a) The $^{13}C/^{12}C$ ratio of dissolved inorganic carbon ($\delta^{13}C$), and (b) seasonally adjusted $\delta^{13}C$. The data have been deseasonalized by fitting the data to harmonics with periods of 12 and 6 months plus a straight line in time by the method of least squares. The slope of the line is -0.025 ± 0.002‰ yr^{-1}. Symbols denote daily averages over the upper 20 m. The error bars denote $\pm$ 1 σ deviations.

surface waters approximately 9 times a year since mid-1983 [*Keeling*, 1993; *Bacastow et al.*, 1996; *Gruber and Keeling*, 1999]. Additional sampling since mid-1990 has taken place at the nearby station of the Bermuda Atlantic Time Series Study (BATS) [*Gruber et al.*, 1998]. The oceanographic characteristics of these two time series sampling sites recently have been summarized by *Michaels and Knap* [1996]. A distinct seasonal oscillation is exhibited by $\delta^{13}C$, with an amplitude, peak to trough, of approximately 0.20-0.30‰ (Figure 11a). About half of the seasonal variability of $\delta^{13}C$ is a result of net community production (defined as net primary production less community respiration), while the remaining variability is due mainly to the combination of air-sea exchange and vertical transport, as shown by *Gruber and Keeling* [1999] and *Gruber et al.* [1998]. Significant interannual variability exists, best seen in the longer data set for Station "S," and evidently related mainly to variations in wintertime vertical overturning of surface water [*Keeling*, 1993; *Bacastow et al.*, 1996].

A negative secular trend in $\delta^{13}C$ is clearly apparent at Station "S." The rate of decrease is somewhat larger in magnitude than the oceanic Suess effect predicted by a three-dimensional oceanic model [*Bacastow et al.*, 1996]. The trend, found by *Bacastow et al.* [1996] to be -0.025 ± 0.002‰ yr^{-1} from 1984 through 1993, has been estimated by fitting the data with a spline curve representing sea-surface winter minimum temperatures, together with a straight line and two seasonal harmonics, with periods of 12 and 6 months. We have here extended this analysis, with two more years of data; fitting the data with only a straight line and two harmonics, we find the same ^{13}C Suess effect to the nearest 0.001‰ ($R^2 = 0.84$) (see Figure 11b). The record is now long enough that this estimate should not be significantly biased by short-term (El Niño-Southern Oscillation (ENSO) timescale) interannual variability, but it may be affected by variability on a decadal time scale, as is known to exist at the station [*Michaels and Knap*, 1996; *Joyce and Robbins*, 1996]. Also, decadal changes

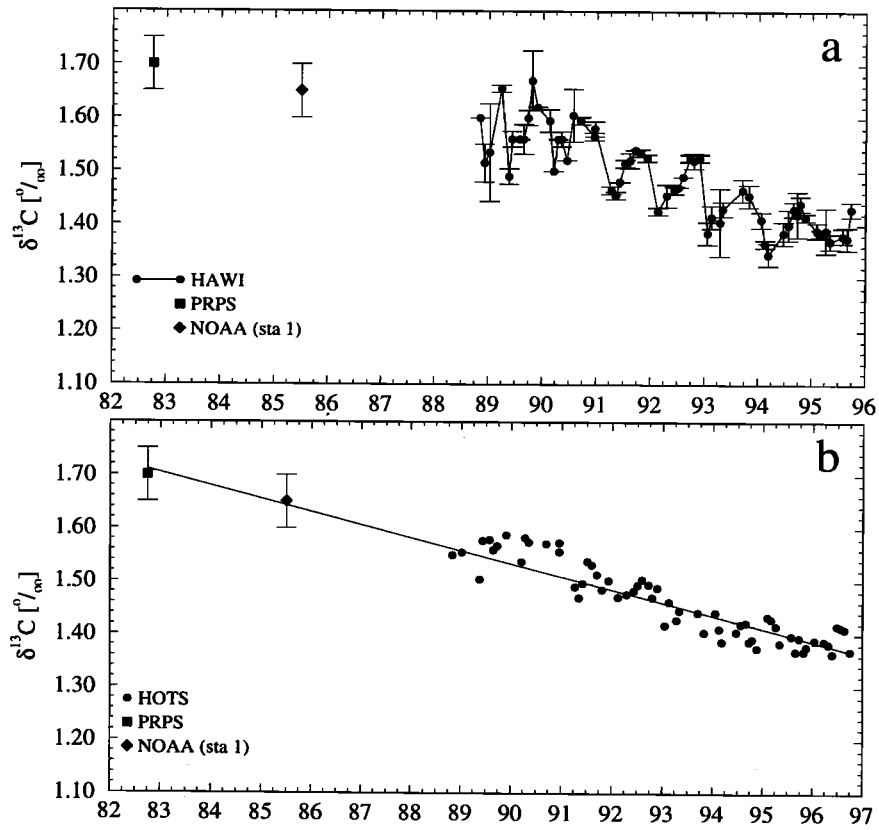

Figure 12. Same as Figure 11, but for the U.S. JGOFS Hawaii Ocean Time Series station (HAWI) at 23°N, 158°W, together with observations made in September 1982 at 21°N, 158°W (PRPS) and in June 1985 at 23°N, 155°W (NOAA). An uncertainty of 0.05‰ has been added to the PRPS and NOAA data points to account for seasonal effects. The line in Figure 12b has been fitted to the combined data by the method of least squares and has a slope of -0.025 ± 0.002‰ yr^{-1}.

in the rate of increase of fossil fuel DIC emmissions will effect the surface water ^{13}C Suess effect, as discussed in section 6.6.

6.2. Time Variations Near Hawaii

Our next most extensive sampling has been at the Hawaii Ocean Time Series study site located at 23°45'N, 158°00'N, north of the island of Oahu (HAWI) (Figure 12). The characteristics of this site are described in detail by *Karl and Lukas* [1996]. The $\delta^{13}C$ record, extending from 1988 through 1996, exhibits in the first year of data a ragged seasonal cycle. After mid-1990, however, the record exhibits a distinct seasonal oscillation with an amplitude, peak to trough, of slightly more than 0.1‰, not quite half as large as that observed near Bermuda. A distinct trend of decreasing $\delta^{13}C$, determined as near Bermuda by a straight line plus two harmonics fit, is found to be -0.030 ± 0.003‰ yr^{-1} ($R^2 = 0.84$). A more precise estimate is obtained, however, by including earlier measurements for September 1982 at 21°N/158°W (PRPS) ($\delta^{13}C = 1.70$‰) and 1985 at 23°N/155°W (NOAA) ($\delta^{13}C = 1.65$‰), yielding a smaller slope of -0.025 ± 0.002‰ yr^{-1} (see Figure 12b). As at the Bermuda stations, this estimate may be affected by interannual variability, especially on a decadal timescale.

6.3. Time Variations in the Central Tropical Pacific

Considerable interannual variability is revealed in surface waters of the central tropical Pacific by repeated meridional transects (Figure 13). Such variability is expected as a consequence of variable intensity and source of upwelling, mainly related to ENSO events. During Benthic Expedition (BNTH), in 1983, with an intense El Niño event in progress, upwelling was practically absent [*Keeling and Revelle*, 1985]. Near the equator, $\delta^{13}C$ values were, on average, 0.4‰ higher, and sDIC was about 60 μmol kg^{-1} lower than typical values. In 1989 on Roundabout Expedition (ROUN), during conditions nearly opposite to those of an El Niño, upwelling was unusually strong. Values lower than typical $\delta^{13}C$

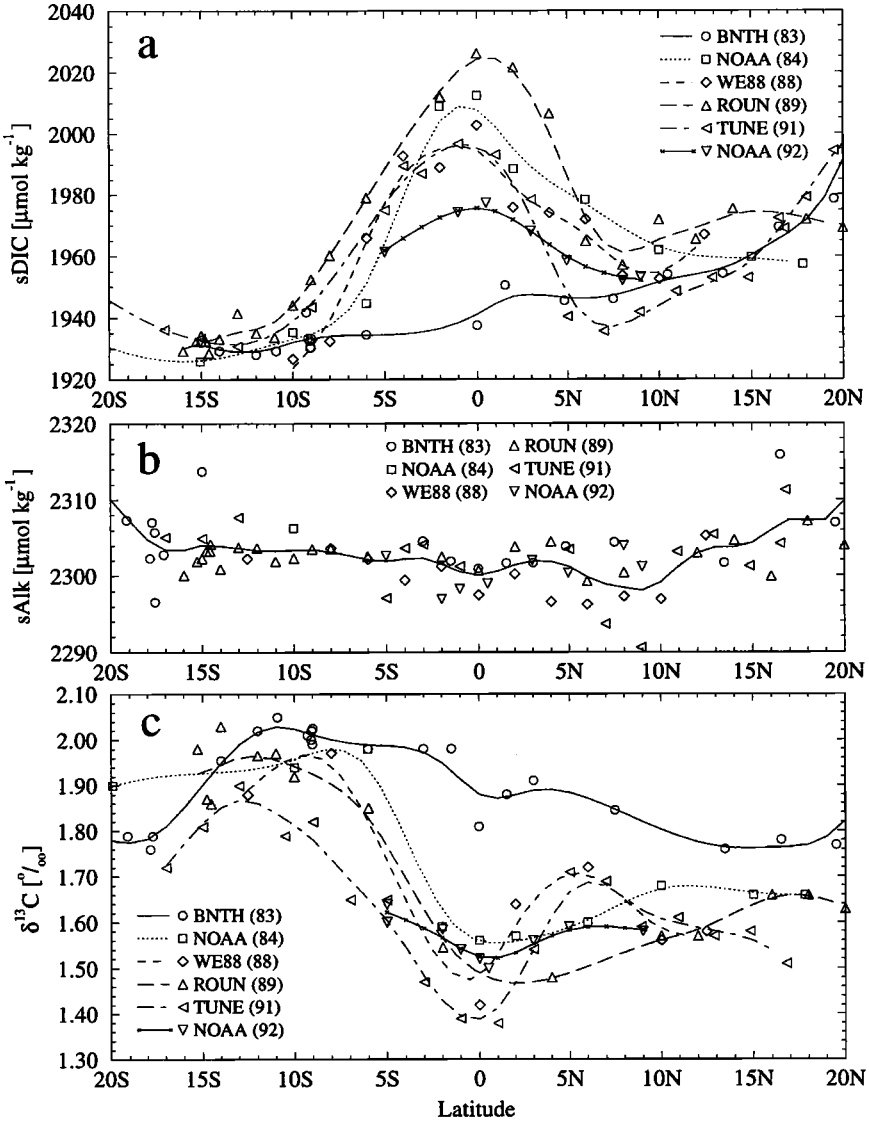

Figure 13. Meridional profiles of inorganic carbon system properties in the upper 50 m of the Central Tropical Pacific Ocean (between 180° and 120°W): (a) normalized dissolved inorganic carbon (sDIC), (b) normalized total alkalinity (sAlk), and (c) the reduced $^{13}C/^{12}C$ ratio of dissolved inorganic carbon ($\delta^{13}C$). Shown are the results of six cruises which sampled the equatorial region between 1983 and 1992. Smoothing splines have been fit to the data of each cruise to emphasize trends. The Benthos Cruise (BNTH) transected the tropical Pacific in 1983 when equatorial upwelling was practically absent owing to an intense El Niño event [*Cane*, 1983].

were observed near the equator, accompanied by higher sDIC. In contrast to sDIC and $\delta^{13}C$, sAlk was nearly constant, as though unaffected by upwelling.

We have established a tentative, secular trend in the Central Tropical Pacific by comparing data for two periods, representing our earliest and our latest transects, from 1979-1980 (FGGE) and from 1993-1995 (TOGA), respectively (Figure 14). The earlier period was characterized by intermediate values of a Southern Oscillation Index (SOI) and nearly normal sea surface temperatures in the region from from 5°S to 5°N and 170° to 120°W, the Niño 3 and 4 regions [*Trenberth and Hoar*, 1997]. The later period was characterized by slightly negative values of the SOI and small positive anomalies in sea surface temperatures in the Niño 3 and 4 regions [*Trenberth and Hoar*, 1996, 1997]. Conditions during these two periods were thus sufficiently similar to estimate a secular trend over 14 years. Although sDIC does not show a significant change (an increase of 5 ± 9 µmol kg^{-1}), a significant decrease of 0.22 ± 0.05‰ is found for

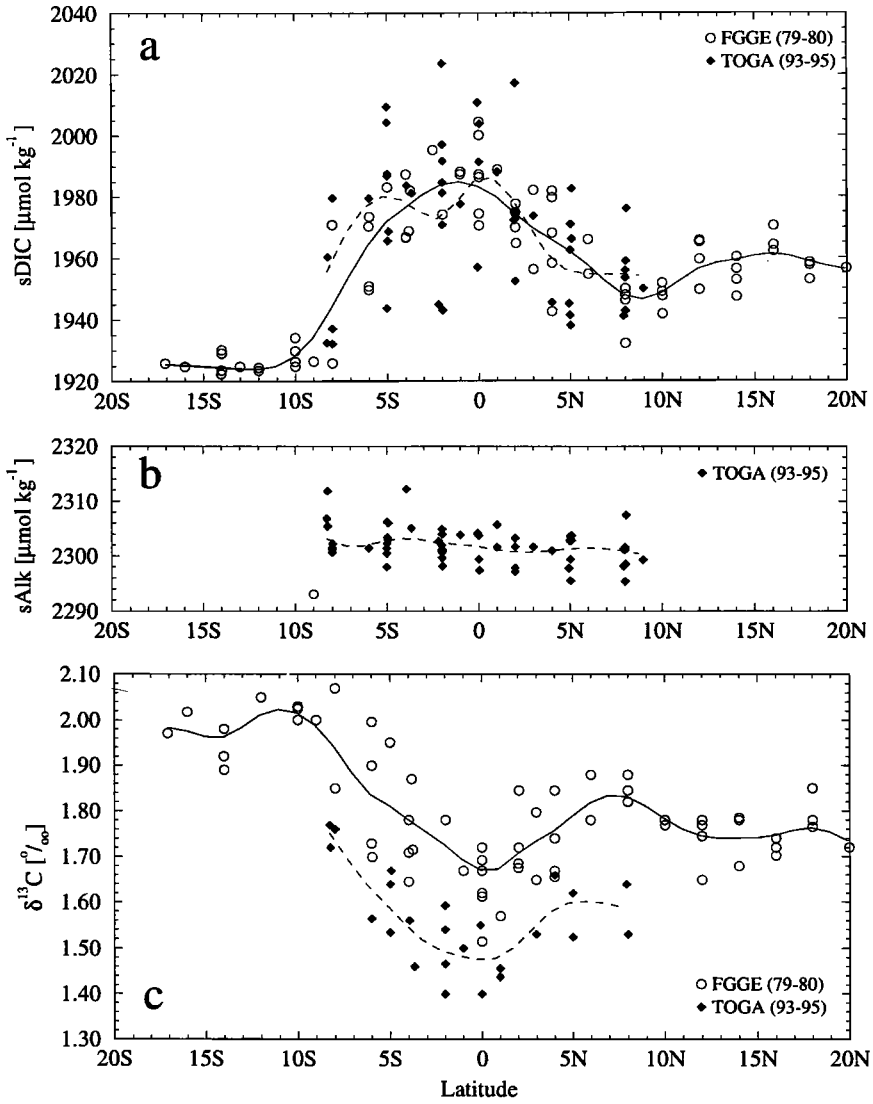

Figure 14. Same as Figure 13, but for results of the FGGE and the TOGA cruises, which sampled the Tropical Ocean in a series of transects between 160° and 150°W during 1979-1980 and 1993-1995, respectively. Between the times of the FGGE and TOGA cruises, a mean δ^{13}C difference of 0.22 ± 0.05‰ is found.

δ^{13}C, leading to a ^{13}C Suess effect of -0.015 ± 0.006‰ yr^{-1}. These changes have been estimated by calculating averages of sDIC and δ^{13}C over six 4° intervals, from 12°S to 12°N, for each cruise, and then calculating the average change. Both programs transected the equator several times during different seasons with both cruises having taken about the same number of samples during Northern Hemisphere summer (May-October) and winter (November-April). We therefore expect that these secular trends should not be affected by a seasonal sampling bias. We also expect that these estimates should not be biased strongly by interannual variability on the ENSO timescale, since the selected sampling periods reflect similar oceanic conditions.

6.4. Secular Changes in the Indian Ocean

Extensive sampling of surface waters of the Indian Ocean on cruises approximately 17 years apart during the GEOSECS program (INDO) in 1978 and the WOCE program (K145) from 1994 to 1996 permits us to investigate secular changes over a wide region from about 40° to 110°E and from 60°S to 20°N (Figure 1d). As noted above, both δ^{13}C and sDIC show significant changes between these expeditions (Figures 4a and 4c). For data from 35°S to 5°N, first averaged over 10° zonal intervals and then averaged again by area (determined by *Gates and Nelson* [1975]), a decrease in δ^{13}C of 0.34 ± 0.07‰ is found. This gives a ^{13}C Suess ef-

Table 2. Summary of Observed ^{13}C Suess Effects in the Surface Ocean

Location	Latitude	Longitude	Time Period	^{13}C Suess Effect,[a] ‰ yr^{-1}
Station "S"	32°N	62°W	1983 - 1996	-0.025 ± 0.002
Station HOT	24°N	158°W	1982 - 1996	-0.025 ± 0.002
Central Tropical Pacific	12°S - 12°N	160°W - 150°W	1979 - 1995	-0.015 ± 0.006
Indian Ocean	35°S - 5°N	40°E - 120°E	1978 - 1995	-0.020 ± 0.004
Global Surface Ocean[b]			1980 - 1995	-0.018

[a]Rate of change of $\delta^{13}C$ of DIC ($d(\delta^{13}C)/dt$).
[b]Extrapolation (see text for details).

fect of -0.020 ± 0.004‰ yr^{-1}. For sDIC, an increase of about 11 ± 9 μmol kg^{-1} is found, thus showing a secular increase of about 0.7 ± 0.5 μmol kg^{-1} yr^{-1}. Because the observed spatial and seasonal variability of $\delta^{13}C$ in the 10° zones is small, these trends should be reasonably representative of the larger zone from 5°N to 35°S. With respect to DIC, we can compare our results to a detailed comparison of surface and subsurface data in a larger data set. Using a multiple correlation technique [*Wallace*, 1995], *Sabine et al.* [1999] found a mean increase of about 16 μmol kg^{-1} between GEOSECS and WOCE in the region north of 35°S, thus a trend of about 1 μmol kg^{-1} yr^{-1}, somewhat higher than we find but in agreement within the uncertainties.

6.5. Global Extrapolation

Table 2 presents a summary of the estimated ^{13}C Suess effects per year in the surface ocean at the three time series locations and in the Indian Ocean, as discussed in sections 6.1-6.4. The highest Suess effect, -0.025‰ yr^{-1}, is found in the subtropical gyres (Bermuda and Hawaii), and the lowest, -0.015‰ yr^{-1}, is found in the equatorial upwelling region in the Pacific. This contrast is consistent with expectations based on the analysis of the oceanic uptake and subsequent redistribution of anthropogenic CO_2 [*Sarmiento et al.*, 1992; *Gruber*, 1998] and bomb radiocarbon [*Broecker et al.*, 1985, 1995]. The surface oceanic ^{13}C Suess effect is predicted to be most pronounced in the subtropical convergence zones, where the invading isotopically light anthropogenic CO_2 tends to accumulate near the ocean surface, whereas in the divergence zones it is diluted by upwelling waters which have little or no anthropogenic CO_2 burden. This pattern is evident in Figure 15. Here we compare estimates of the ^{13}C Suess effect based on our data with estimates which we have made on basis of data of *Kroopnick et al.* [1977] and *Quay et al.* [1992]. The data of *Kroopnick et al.* [1977] stem from the Canadian HUDSON-70 cruise in 1970 along 150°W between 65°S and 55°N. *Quay et al.* [1992] regard these data to be more reliable than the GEOSECS $\delta^{13}C$ data of *Kroopnick* [1985]. The data of *Quay et al.* [1992] stem from three research cruises of the National Oceanographic and Atmospheric Administration between 1989 and 1991 in the central and eastern Pacific between 60°S and 60°N. We have calculated the ^{13}C Suess effect from Kroopnick and Quay's data by first computing zonal averages at 10° intervals for each time period (1970 and 1989-1991) and then dividing the differences between periods by the mean time difference of 20 years. Estimates based on our data at 24°N and near the equator in the Pacific Ocean agree well with the estimates from the 10° zonal averages derived from the data of *Kroopnick et al.* [1977] and *Quay et al.* [1992]. Analogous to anthropogenic CO_2 and bomb radiocarbon data, the meridional pattern of the ^{13}C Suess effect in the other ocean basins is expected to be similar to that exhibited in the Pacific. This view is supported by our ^{13}C Suess effect estimates obtained near Bermuda and in the tropical and subtropical Indian ocean (Figure 15). The three-dimensional carbon cycle model simulation by *Bacastow et al.* [1996] further supports this assumption.

If we therefore assume that the meridional distributions of $\delta^{13}C$ in all ocean basins are similar, we can extrapolate our estimates of the surface ocean ^{13}C Suess to the global surface ocean. To obtain a tentative global $\delta^{13}C$ Suess effect, let us assume that the effect north of 35°S is of the order of -0.020‰ yr^{-1}, on the basis of the average value found in the Indian ocean from 35°S to 5°N. (The same value is obtained in the Pacific by averaging the Suess effect found in the subtropics near Hawaii and that found near the equator). Let us further assume that the ^{13}C Suess effect decreases linearly south of 35°S to -0.002‰ yr^{-1} at 80°S. This is a somewhat smaller decrease toward Antarctica than suggested by the data of *Quay et al.* [1992] and *Kroopnick et al.* [1977] but more in accordance with our Indian Ocean data (Figure 4c). We thus arrive at a global ocean surface estimate for the ^{13}C Suess effect of about -0.018‰ yr^{-1} for the period from approximately 1980 to 1995 based on our own data. A similar estimate,

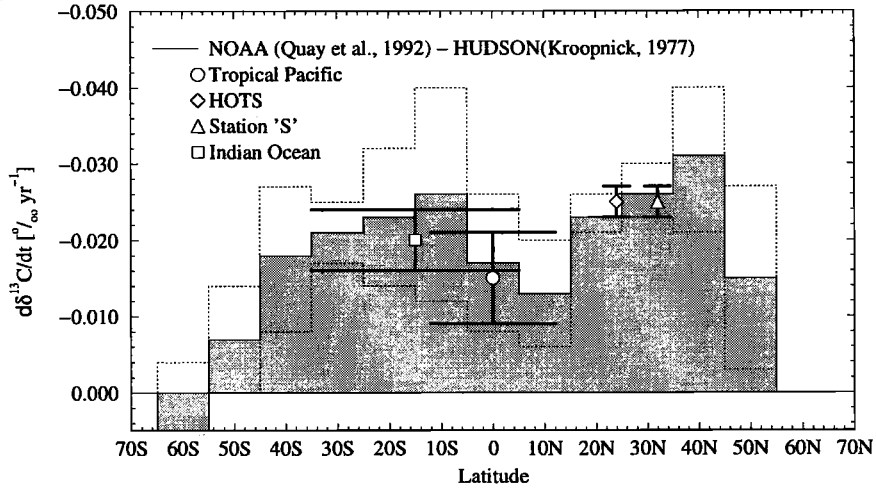

Figure 15. Meridional variability in estimated ^{13}C Suess effects in the surface waters. The scale has been inverted so that a positive Suess effect is plotted upward. The symbols denote estimates derived in this study from time series locations near Bermuda (Station "S" (triangle)), near Hawaii (HOTS (diamond)), the central tropical Pacific (circle), and the tropical and subtropical Indian Ocean (square). Vertical error bars denote the uncertainties; horizontal bars show the areal extent over which the estimate has been obtained. Also shown, as shaded bars, are 10° meridional means of the ^{13}C Suess effect estimated from the data of *Kroopnick et al.* [1977], obtained in 1970 along 150°W, and from data of *Quay et al.* [1992], obtained between 1989 and 1991 during three separate meridional NOAA cruises in the central and eastern Pacific. The dashed lines represent ± 1 standard deviation of these estimates.

-0.017 ± 0.002‰ yr^{-1}, is obtained using the zonal averages calculated from the Pacific ocean data of *Quay et al.* [1992] and *Kroopnick et al.* [1977] weighted by surface ocean area. The uncertainty of our global extrapolation cannot be established, but it is encouraging to note that these two independent estimates are close to the global surface ocean average ^{13}C Suess effect of -0.017‰ yr^{-1} (1983-1995) predicted by the three-dimensional carbon cycle model employed by *Bacastow et al.* [1996].

6.6. Comparison of Oceanic and Atmospheric Suess Effect

During the period 1980-1995, atmospheric $\delta^{13}C$ decreased on average at a rate of approximately -0.018 ± 0.001‰ yr^{-1}, according to a linear regression of data for

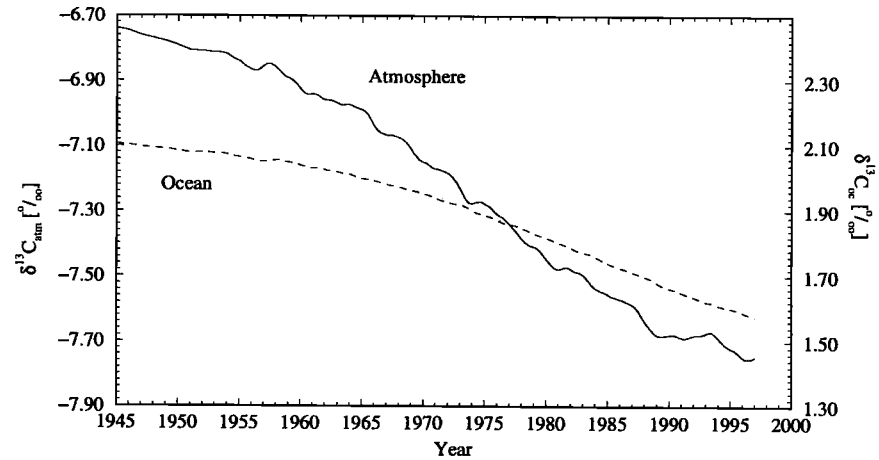

Figure 16. Box-diffusion model prediction of atmospheric and surface ocean ^{13}C Suess effects. The model, as implemented by *Keeling et al.* [1989], was run in the single deconvolution mode with parameters set by *Keeling et al.* [1989, Table 8, p. 189] (bomb ^{14}C calibration). In this mode, measured atmospheric CO_2 concentration and estimated industrial CO_2 production and its reduced ratio $\delta^{13}C$ are input to the model. Atmospheric and oceanic $\delta^{13}C$ are predicted.

Mauna Loa, Hawaii, and the South Pole, as seasonally adjusted and combined by *Keeling et al.* [1995]. The estimated global oceanic ^{13}C Suess effect is therefore approximately equal to the atmospheric Suess effect over the period of measurement. This may at first seem surprising, since one would expect the ^{13}C change in the surface ocean to be smaller than the ^{13}C change in the atmosphere, which is the driving reservoir. The ratio of these effects on the timescale of decades and longer has been estimated to be approximately 0.6 [*Keeling*, 1979] and 0.7 [*Broecker and Peng*, 1993]. These low model-based ratios are supported by the $\delta^{13}C$ proxy measurements on sponges by *Böhm et al.* [1996]. They obtained a cumulative Suess effect of about −0.7‰ to −0.9‰ up to 1992 at two warm water locations, which, when compared to the atmospheric cumulative Suess effect, gives a ratio of 0.5-0.6.

However, it is clear that the effect depends strongly on the rate of growth of the anthropogenic CO_2 input to the atmosphere [*Keeling*, 1979]. Fossil fuel CO_2 input has increased approximately exponentially at a rate of growth, r, of 0.042 yr^{-1} from 1948 to 1979, but since then the increase has been more erratic, with hesitations or decreases from 1979 to 1984, and 1990 to 1995. The average growth rate from 1979 to 1997 was about 0.011 yr^{-1}.

After times long compared to $1/r$, CO_2 perturbations in a globally averaged model will increase in each reservoir at an exponential rate with rate constant r [*Bacastow and Keeling*, 1979]. It can be shown that the ^{13}C perturbations will also increase at the same exponential rate. A reduction in r would be expected first to reduce the Suess effect in the atmosphere and then also in the ocean but with a considerable time lag because of the 10 year equilibration time for ^{13}C between the atmosphere and surface ocean. This behavior is seen in box-diffusion model predictions of the atmosphere and surface ocean Suess effects (Figure 16). The model was run in the single deconvolution mode, in which the measured atmospheric CO_2 concentration is input to the model along with fossil fuel CO_2, while the $\delta^{13}C$ histories in the surface ocean and the atmosphere are calculated prognostically. The atmospheric Suess effect is predicted to decrease to a value near that of the oceanic effect for the period 1980-1995. The oceanic effect is also predicted to decrease, but not by as much, presumably because of the aforementioned lag.

7. Summary and Conclusions

The $\delta^{13}C$ distribution in the surface ocean is governed by the interaction of biological and thermodynamic processes which have strong opposing influences. Biological processes influence $\delta^{13}C$ because the phytoplankton preferentially takes up the lighter isotope ^{12}C over ^{13}C during the photosynthetic fixation of CO_2. Thermodynamic processes influence isotopic fractionations mainly through air-sea exchange because the $\delta^{13}C$ of DIC in isotopic equilibrium with the atmosphere is strongly temperature dependent, tending to make the $\delta^{13}C$ values in cold waters higher than those in warm waters via air-sea exchange.

The balance between these two influences leads to a complex surface distribution pattern with relatively slight variability. Distinct features can nevertheless be found in all ocean basins. Most prominent are a maximum of $\delta^{13}C$ near the subantarctic front and low values in the Southern Ocean. The former is mainly caused by the strong fractionation that occurs during photosynthetic fixation of CO_2, tempered by air-sea exchange. The latter reflects the upwelling of waters in the Southern Ocean with high concentrations of remineralized organic matter, also tempered by air-sea exchange. The low latitudes show little variability, except downstream of upwelling regions where the biological uptake of isotopically light CO_2, fertilized by upwelled nutrient-rich water, creates distinct maxima. Air-sea exchange tends to lower $\delta^{13}C$ in these regions. The extent of its influence depends on the mean residence time of waters near the surface, since the equilibration time for the ^{13}C isotope is about 10 years. Lowest values can therefore be found in the centers of the subtropical gyres, where biological activity is low and waters stay for a long time in contact with the atmosphere.

Observations at three time series stations and a repeated survey in the Indian Ocean permit us to estimate secular decreases of $\delta^{13}C$ caused by the addition of anthropogenic CO_2 to the atmosphere (^{13}C Suess effect). A tentative extrapolation of the secular decreases in $\delta^{13}C$ to the global surface ocean results in a ^{13}C Suess effect of the order of $-0.018‰\ yr^{-1}$ for the period from 1980 to 1995, nearly the same as that in the atmosphere for the same period. This is consistent with a box diffusion model prediction of the oceanic and atmospheric Suess effect during this period and is apparently due to a reduction in the exponential growth rate of anthropogenic CO_2.

Appendix A: Measurement Methods

Duplicate samples of seawater were collected following the procedures described by *Lueker* [1998]. The bottles were shipped to the laboratory of the Carbon Dioxide Research Group (CDRG) of the Scripps Institution of Oceanography, where they were stored in the dark until analysis. Measurement procedures for dissolved inorganic carbon and total titration alkalinity (Alk) are given in detail by *Lueker* [1998] and for the $^{13}C/^{12}C$ ratio of DIC as described below. Briefly, DIC was measured by a cryogenic vacuum extraction followed by a manometric determination of the amount of

evolved CO_2 gas. The precision of replicate determinations of DIC in the laboratory is about ± 0.5 μmol kg^{-1}. The accuracy is estimated to be about ± 1.0 μmol kg^{-1}. Alk was determined using a closed cell titration with an estimated precision from replicate determinations of ± 1.0 μmol kg^{-1} and an accuracy of about ± 5 μmol kg^{-1}. The $^{13}C/^{12}C$ ratio of DIC was determined on the same extracted CO_2 gas as used for the manometric measurement of DIC. After the manometric measurement, the CO_2 gas was quantitatively collected cryogenically and sealed by flame in glass tubes. Samples extracted before October 1992 were shipped to the Centre for Isotope Physics (CIO) of Groningen University where mass spectrometric analysis of the $^{13}C/^{12}C$ ratio was carried out using a VG micromass 903 isotope ratio mass spectrometer prior to 1986 and a VG SIRA 9 after that. Daily calibrations were based on a suite of carbonate and pure CO_2 standards [*Roeloffzen*, 1993]. These standards were repeatedly calibrated against primary standards from the National Bureau of Standards (NBS 18, NBS 19, and VSMOW). No N_2O correction was applied to sea water samples. After October 1992, extracted samples were analyzed at the Isotope Laboratory of the Scripps Institution of Oceanography using a VG Prism II isotope mass spectrometer. Daily calibrations, based on six secondary standards, were applied to the data, as described by *Bollenbacher et al.* [1998]. The six secondary standards consisted of three standards prepared at SIO by extracting CO_2 from air stored under high pressure in steel cylinders, two standards supplied by CIO (GS19 and GS20), and one standard prepared from sodium bicarbonate at SIO. These standards were calibrated against primary standards of CO_2 derived from international isotopic standards of the National Bureau of Standards (NBS-16, NBS-17, and NBS-19).

To measure small changes in the $^{13}C/^{12}C$ ratio of DIC, one must be concerned about discontinuities in procedure and in long-term drift of the mass spectrometer used in the measurements. The change between analysis at CIO and SIO was examined by analyzing samples of three sodium bicarbonate solution standards as well as a set of samples extracted from surface sea water collected off southern California [*Bollenbacher et al.*, 1998]. On average, the SIO measurements were greater by 0.016‰ than measurements made at CIO, a difference too small to justify applying an adjustment.

We report the $^{13}C/^{12}C$ isotopic ratio of DIC as the reduced ratio, $\delta^{13}C$, defined by

$$\delta^{13}C = \frac{{}^{13}r - {}^{13}r_s}{{}^{13}r_s}, \tag{A1}$$

where ${}^{13}r$ denotes the $^{13}C/^{12}C$ ratio of the sample, and ${}^{13}r_s$ denotes the $^{13}C/^{12}C$ ratio of Pee Dee belemnite standard [*Craig*, 1957; *Mook and Grootes*, 1973]. Since the values of $\delta^{13}C$ are small, they are expressed in per mil (‰). The precision and accuracy of the $\delta^{13}C$ analyses are estimated to be ± 0.02‰and ± 0.05‰, respectively.

Our replicate sampling strategy permits us also to estimate the sampling error under the assumption that the analysis errors remain constant and that the two errors are uncorrelated. We found that the sampling errors vary strongly with cruises with a mean of 0.7 μmol kg^{-1} for DIC, 1.1 μmol kg^{-1} for Alk, and 0.03‰ for $\delta^{13}C$. This results in a typical combined error (analysis and sampling error) of 0.9 μmol kg^{-1} for DIC, 1.5 μmol kg^{-1} for Alk, and 0.04‰ for $\delta^{13}C$.

Appendix B: Derivation of $\delta^{13}C^*$

For the derivation of $\delta^{13}C^*$, we will largely follow *Gruber et al.* [1996] in their derivation of the conservative tracer C^*. We will derive a conservative tracer for $DI^{13}C$, analogous to C^*, which will be named ${}^{13}C^*$. The ratio of ${}^{13}C^*$ to C^*, in the δ notation, is then expressed as $\delta^{13}C^*$.

The cycling of DIC ($DI^{12}C + DI^{13}C$) and $DI^{13}C$ are controlled by air-sea exchange at the surface (solubility pump), the biological processes of photosynthesis, respiration, and remineralization (soft-tissue pump), as well as the formation and dissolution of carbonate particles (carbonate pump). The latter represents the main controlling process for alkalinity (Alk). Alk is also affected by the soft-tissue pump due to a proton flux associated with the redox reactions between reduced organic nitrogen and nitrate [*Brewer et al.*, 1975]. By contrast, the biogeochemical cycling of phosphate is entirely governed by the soft-tissue pump. The tracer continuity equations for DIC, $DI^{13}C$, Alk, and PO_4 can therefore be written as

$$\Gamma(\mathrm{DIC}) = J_{\mathrm{soft}}(\mathrm{DIC}) + J_{\mathrm{carb}}(\mathrm{DIC}), \tag{B1}$$

$$\Gamma(\mathrm{DI^{13}C}) = J_{\mathrm{soft}}(\mathrm{DI^{13}C}) + J_{\mathrm{carb}}(\mathrm{DI^{13}C}), \tag{B2}$$

$$\Gamma(\mathrm{Alk}) = J_{\mathrm{soft}}(\mathrm{Alk}) + J_{\mathrm{carb}}(\mathrm{Alk}), \tag{B3}$$

$$\Gamma(\mathrm{PO_4}) = J_{\mathrm{soft}}(\mathrm{PO_4}), \tag{B4}$$

where J_{soft} denotes the source term due to the formation and remineralization of organic matter and J_{carb} denotes the source term due to the production and dissolution of carbonate particles. The operator Γ represents the transport and time rate of change:

$$\Gamma(T) = \frac{\partial T}{\partial t} + \vec{u} \cdot \nabla T - \nabla \cdot (D \cdot \nabla T), \tag{B5}$$

where T is any tracer concentration, ∇ represents the gradient operator in three dimensions, $\vec{u}$ denotes the velocity field, and D is the eddy diffusivity tensor.

We assume that the soft-tissue pump influences DIC and PO_4 with a constant atomic ratio ($r_{C:P}$), and that the carbonate pump changes alkalinity twice as much as it changes DIC. The proton flux during the processes of photosynthesis, respiration, and remineralization is assumed to be proportional to the change in the nitrate concentration, which in turn is proportional to the change in PO_4 through the constant atomic ratio $r_{N:P}$ thus

$$J_{\text{soft}}(\text{DIC}) = r_{C:P} J_{\text{soft}}(\text{PO}_4), \tag{B6}$$

$$J_{\text{carb}}(\text{DIC}) = \tfrac{1}{2} J_{\text{carb}}(\text{Alk}), \tag{B7}$$

$$J_{\text{soft}}(\text{Alk}) = -J_{\text{soft}}(\text{NO}_3) = -r_{N:P} J_{\text{soft}}(\text{PO}_4). \tag{B8}$$

We further assume that the soft-tissue pump produces organic matter with a constant $^{13}\text{C}/(^{13}\text{C}+^{12}\text{C})$ ratio, $^{13}R_{\text{org}}$, and that organisms produce carbonate shells with a constant $^{13}\text{C}/(^{13}\text{C}+^{12}\text{C})$ ratio, $^{13}R_{\text{carb}}$,

$$J_{\text{soft}}(\text{DI}^{13}\text{C}) = {}^{13}R_{\text{org}} J_{\text{soft}}(\text{DIC}), \tag{B9}$$

$$J_{\text{carb}}(\text{DI}^{13}C) = {}^{13}R_{\text{carb}} J_{\text{carb}}(\text{DIC}). \tag{B10}$$

Substituting (B6)-(B10) into equations (B1)-(B3) gives

$$\Gamma(\text{DIC}) = r_{C:P} J_{\text{soft}}(\text{PO}_4) + \tfrac{1}{2} J_{\text{carb}}(\text{Alk}), \tag{B11}$$

$$\Gamma(\text{DI}^{13}\text{C}) = {}^{13}R_{\text{org}} r_{C:P} J_{\text{soft}}(\text{PO}_4) + \tfrac{1}{2}{}^{13}R_{\text{carb}} J_{\text{carb}}(\text{Alk}), \tag{B12}$$

$$\Gamma(\text{Alk}) = -r_{N:P} J_{\text{soft}}(\text{PO}_4) + J_{\text{carb}}(\text{Alk}). \tag{B13}$$

We can eliminate the $J_{\text{soft}}(\text{PO}_4)$ and $J_{\text{carb}}(\text{Alk})$ terms from equation (B11) by subtracting $r_{C:P}\Gamma(\text{PO}_4)$ and $\frac{1}{2}(\Gamma(\text{Alk}) + r_{N:P}\Gamma(\text{PO}_4))$ from it. Similarly these two terms can be eliminated from the DI^{13}C equation (B12) by subtracting $r_{C:P}{}^{13}R_{\text{org}}\Gamma(\text{PO}_4)$ and $\frac{1}{2}{}^{13}R_{\text{carb}}(\Gamma(\text{Alk}) + r_{N:P}\Gamma(\text{PO}_4))$. This yields

$$\Gamma(\text{DIC}) - r_{C:P}\Gamma(\text{PO}_4) - \tfrac{1}{2}(\Gamma(\text{Alk}) + r_{N:P}\Gamma(\text{PO}_4)) = 0, \tag{B14}$$

$$\Gamma(\text{DI}^{13}C) - r_{C:P}{}^{13}R_{\text{org}}\Gamma(\text{PO}_4) - \tfrac{1}{2}{}^{13}R_{\text{carb}}(\Gamma(\text{Alk}) + r_{N:P}\Gamma(\text{PO}_4)) = 0. \tag{B15}$$

Since the atomic ratios and the isotopic ratios of organic matter and calcium carbonates are assumed to be constant and since the operator Γ is linear, the terms outside the operators can be taken inside and the different operators combined. This permits us to define two new tracers C^* and $^{13}C^*$,

$$C^* = \text{DIC} - r_{C:P}\text{PO}_4 - \tfrac{1}{2}(\text{Alk} + r_{N:P}\text{PO}_4) + \text{const}, \tag{B16}$$

$$^{13}C^* = DI^{13}C - r_{C:P}{}^{13}R_{\text{org}}\text{PO}_4 - \tfrac{1}{2}{}^{13}R_{\text{carb}}(\text{Alk} + r_{N:P}\text{PO}_4) + \text{const}, \tag{B17}$$

with conservative properties

$$\Gamma(C^*) = 0, \tag{B18}$$

$$\Gamma(^{13}C^*) = 0. \tag{B19}$$

The definition of C^* here differs from that given by *Gruber et al.* [1996] in that (1) phosphate instead of oxygen is used to remove the contribution of biological processes and (2) a constant is additionally considered. We chose to use phosphate here because we are primarily interested in the imprint of air-sea gas exchange and solubility on DIC and DI^{13}C. In the case in which C^* is defined using oxygen as a tracer, the strong temperature dependency of oxygen solubility masks this imprint. This complication can be avoided by using phosphate in place of oxygen.

We determine the constants in equations (B16) and (B17) by requiring that the values of C^* and $^{13}C^*$ are similar in magnitude to DIC and DI^{13}C. This is the case if we set the constants equal to $r_{C:P}\text{PO}_4^o + \frac{1}{2}(\text{Alk}^o - r_{N:P}\text{PO}_4^o)$ with respect to C^* and equal to $r_{C:P}{}^{13}R_{\text{org}}\text{PO}_4^o + \frac{1}{2}{}^{13}R_{\text{carb}}(\text{Alk}^o - r_{N:P}\text{PO}_4^o)$ with respect to $^{13}C^*$, where PO_4^o and Alk^o are constant reference values. This gives

$$C^* = \text{DIC} - r_{C:P}\Delta\text{PO}_4 - \tfrac{1}{2}(\Delta\text{Alk} + r_{N:P}\Delta\text{PO}_4), \tag{B20}$$

$$^{13}C^* = \text{DI}^{13}\text{C} - r_{C:P}{}^{13}R_{\text{org}}\Delta\text{PO}_4 - \tfrac{1}{2}{}^{13}R_{\text{carb}}(\Delta\text{Alk} + r_{N:P}\Delta\text{PO}_4), \tag{B21}$$

where $\Delta\text{PO}_4 = \text{PO}_4 - \text{PO}^o$ and $\Delta\text{Alk} = \text{Alk} - \text{Alk}^o$.

Next it is instructive to look at the ratio of $^{13}C^*$ to C^*, $^{13}R^*$:

$$^{13}R^* = \frac{\text{DIC}}{C^*}\left({}^{13}R - \frac{r_{C:P}{}^{13}R_{\text{org}}}{\text{DIC}}\Delta\text{PO}_4 - \frac{{}^{13}R_{\text{carb}}}{2\,\text{DIC}}(\Delta\text{Alk} + r_{N:P}\Delta\text{PO}_4)\right). \tag{B22}$$

It is important to note that $^{13}R^*$ is not strictly conservative. However, variations in DIC due to biological processes are relatively small compared to the absolute value of DIC (up to 20%), so that deviations of $^{13}R^*$ from a conservative behavior remain relatively small. In δ notation:

$$^{13}R = {}^{13}R_s\left(\delta^{13}\text{C} + 1\right). \tag{B23}$$

Hence

$$\delta^{13}C^* = \frac{\text{DIC}}{C^*}\left(\delta^{13}\text{C} - \frac{r_{C:P}\delta^{13}C_{\text{org}}}{\text{DIC}}\Delta\text{PO}_4 - \frac{\delta^{13}C_{\text{carb}}}{2\,\text{DIC}}(\Delta\text{Alk} + r_{N:P}\Delta\text{PO}_4)\right). \tag{B24}$$

Making three additional assumptions, the expression $\delta^{13}C^*$ can be simplified to yield the quantity $\delta^{13}C_{\text{as}}$

as defined by *Lynch-Stieglitz et al.* [1995]:

$$\delta^{13}C_{as} = \delta^{13}\mathrm{C} - \frac{r_{C:P}\delta^{13}C_{\mathrm{org}}}{\overline{\mathrm{DIC}}}\Delta\mathrm{PO_4} + \mathrm{const}, \quad \text{(B25)}$$

where $\overline{\mathrm{DIC}}$ denotes the mean ocean DIC concentration.

These assumptions are (1) variations in DIC due to the biological pumps are much smaller than DIC, so that $\mathrm{DIC}/C^* \approx 1$. (2) The contribution of the carbonate pump is small and can therefore be neglected. (3) Variations in DIC are small and therefore DIC can be replaced by the ocean mean DIC ($\overline{\mathrm{DIC}}$). Inserting the values chosen by *Lynch-Stieglitz et al.* [1995] for $r_{C:P}$ (128), for $\delta^{13}C_{\mathrm{org}}$ (−20‰), for $\overline{\mathrm{DIC}}$ (2200 μmol kg^{-1}), and for $\mathrm{PO_4^o}$ (2.2 μmol kg^{-1}) and adjusting the constant to reflect their estimate of the mean ocean δ^{13}C of 0.3‰yields the final definition for $\delta^{13}C_{\mathrm{as}}$:

$$\delta^{13}C_{as} = \delta^{13}\mathrm{C} + 1.1\ ‰\ \mu\mathrm{mol}^{-1}\ \mathrm{kg}\ \mathrm{PO_4} - 2.7\ ‰. \quad \text{(B26)}$$

Acknowledgments. We are deeply indebted to the members of the Carbon Dioxide Research Group at the Scripps Institution of Oceanography who were responsible for sampling, measurement, and management of the data employed in this study. These are namely G. Emanuele, A. Bollenbacher, K. Egan, B. Stewart, and D. Moss. This work would not have been possible without the great help of the numerous scientists and personnel who collected water samples for us during the many different oceanographic cruises. The work of the first author was supported by a postdoctoral fellowship from the Swiss National Science Foundation. The Swiss National Science Foundation also granted support for TFS. The measurements at the University of Groningen were in part supported by the "Disturbance of Earth Systems" project of the Netherlands Geosciences Foundation (GOA) with financial aid from the Netherlands Organization for Scientific Research (NWO). Costs of this study borne by the Scripps Institution of Oceanography were funded by a series of grants from the U.S. National Science Foundation, U.S. Department of Energy, and U.S. National Aeronautics and Space Administration; the more recent grants being NSF ATM-9121986, NSF ATM-9711882, OCE-9725955, DE-FG03-90ER60940, DE-FG03-93ER61543, DE-FG03-95ER62075, and NASA NAG5-3528.

References

Anderson, L. A., and J. Sarmiento, Global ocean phosphate and oxygen simulations, *Global Biogeochem. Cycles, 9*(4), 621–636, 1995.

Andres, R. J., G. Marland, and S. Bischoff, Global and latitudinal estimates of δ^{13}C from fossil fuel consumption and cement manufacture, *Carbon Dioxide Inf. Anal. Cent., CDIAC Communications, 22*, Oak Ridge Natl. Lab., Oak Ridge, Tenn., 1996.

Bacastow, R., and C. Keeling, Models to predict future atmospheric CO_2 concentrations, in *Workshop on the Global Effects of Carbon Dioxide from Fossil Fuels*, edited by W. P. Elliott and L. Machta, pp. 72–90, U. S. Dep. of Energy, Washington, D.C., 1979.

Bacastow, R. B., C. D. Keeling, T. J. Lueker, M. Wahlen, and W. G. Mook, The ^{13}C Suess effect in the world surface oceans and its implications for oceanic uptake of CO_2: Analysis of observations at Bermuda, *Global Biogeochem. Cycles, 10*(2), 335–346, 1996.

Böhm, F., M. Joachimski, H. Lehnert, G. Morgenroth, W. Kretschmer, J. Vacelet, and W.-C. Dullo, Carbon isotope records from extant Caribbean and South Pacific sponges: Evolution of $\delta^{13}C$ in surface water DIC, *Earth Planet. Sci. Lett., 139*, 291–303, 1996.

Bollenbacher, A. F., C. D. Keeling, E. F. Stewart, M. Wahlen, and T. P. Whorf, Calibration methodology for the Scripps $^{13}C/^{12}C$ and $^{18}O/^{16}O$ stable isotope program, tech. rep., Scripps Inst. of Oceanogr., La Jolla, Calif., 1998.

Brewer, P., G. Wong, M. Bacon, and D. Spencer, An oceanic calcium problem?, *Earth Planet. Sci. Lett., 26*, 81–87, 1975.

Brewer, P. G., A. L. Bradshaw, and R. T. Williams, Measurements of total carbon dioxide and alkalinity in the North Atlantic in 1981, in *The Changing Carbon Cycle*, edited by J. R. Trabalka and R. E. Reichle, pp. 348–370, Springer-Verlag, New York, 1986.

Broecker, W. S., "NO": A conservative water-mass tracer, *Earth Planet. Sci. Lett., 23*, 100–107, 1974.

Broecker, W. S., and E. Maier-Reimer, The influence of air and sea exchange on the carbon isotope distribution in the sea, *Global Biogeochem. Cycles, 6*(3), 315–320, 1992.

Broecker, W. S., and T. H. Peng, Gas exchange rates between air and sea, *Tellus, 26*, 21–35, 1974.

Broecker, W. S., and T.-H. Peng, *Tracers in the Sea*, Eldigio, Lamont-Doherty Geol. Obs., Palisades, N.Y., 1982.

Broecker, W. S., and T.-H. Peng, Evaluation of the ^{13}C constraint on the uptake of fossil fuel CO_2 by the ocean, *Global Biogeochem. Cycles, 7*(3), 619–626, 1993.

Broecker, W. S., T. H. Peng, G. Ostlund, and M. Stuiver, The distribution of bomb radiocarbon in the ocean, *J. Geophys. Res., 90*(C4), 6953–6970, 1985.

Broecker, W. S., S. Sutherland, W. Smethie, T.-H. Peng, and G. Ostlund, Oceanic radiocarbon: Separation of the natural and bomb components, *Global Biogeochem. Cycles, 9*(2), 263–288, 1995.

Cane, M. A., Oceanographic events during El Niño, *Science, 222*, 1189–1195, 1983.

Charles, C. D., and R. G. Fairbanks, Glacial to interglacial ^{13}C change in benthic and planctonic foraminifera from the Southern Oceans, in *Geological History of the Polar Oceans: Arctic Versus Antarctic*, edited by U. Bleil and J. Thiede, pp. 512–538, Kluwer Acad., Norwell, Mass., 1990.

Charles, C. D., J. D. Wright, and R. G. Fairbanks, Thermodynamic influences on the marine carbon isotope record, *Paleoceanography, 8*(6), 691–697, 1993.

Craig, H., Isotopic standards for carbon and oxgyen and correction factors for mass-spectrometric analysis of carbon dioxide, *Geochim. Cosmochim. Acta, 12*, 133–149, 1957.

Curry, W. B., J. C. Duplessy, L. D. Labeyrie, and N. J. Shackelton, Changes in the distribution of δ^{13}C of deep water TCO_2 between the last glaciation and the holocene, *Paleoceanography, 3*(3), 317–341, 1988.

Duplessy, J. C., N. J. Shackelton, R. K. Matthews, W. Prell, W. F. Ruddiman, M. H. Caralp, and C. H. Hendy, ^{13}C record of benthic foraminifera in the last interglacial ocean: implications for the carbon cycle and the global deep water circulation, *Quat. Res., 21*, 225–243, 1984.

Fink, R., *Zur Kohlenstoffchemie des Ozeans und zur Model-*

lierung des natürlichen Kohlenstoffkreislaufes, Ph. D. thesis, Phys. Inst., Univ. of Bern, Bern, Switzerland, 1996.

Francey, R. J., C. E. Allison, D. M. Etheridge, C. M. Trudinger, I. G. Enting, M. Leuenberger, R. L. Langenfelds, E. Michel, and L. P. Steele, A 1000 year high precision record of $\delta^{13}C$ in atmospheric CO_2, *Tellus, Ser. B.*, in press, 1998.

Freeman, K. H., and J. M. Hayes, Fractionation of carbon isotopes by phytoplankton and estimates of ancient CO_2 levels, *Global Biogeochem. Cycles, 6*(2), 185–198, 1992.

Friedli, H., H. Loetscher, H. Oeschger, U. Siegenthaler, and B. Stauffer, Ice core record of the $^{13}C/^{12}C$ ratio of atmospheric CO_2 in the past two centuries, *Nature, 324*, 237–238, 1986.

Gates, W., and A. Nelson, A new (revised) tabulation of the Scripps topography on a 1 degree global grid., in *Tech. Rep. II: Ocean depths*, Rand Corp., Santa Monica, Calif., 1975.

Goericke, R., and B. Fry, Variations of marine plankton $\delta^{13}C$ with latitude, temperature, and dissolved CO_2 in the world ocean, *Global Biogeochem. Cycles, 8*(1), 85–90, 1994.

Gordon, A. L., Spatial and temporal variability within the Southern Ocean, in *Antarctic Ocean and Resources Variability*, edited by D. Sahrhage, pp. 41–56, Springer-Verlag, New York, 1988.

Gruber, N., Anthropogenic CO_2 in the Atlantic Ocean, *Global Biogeochem. Cycles, 12*(1), 165–191, 1998.

Gruber, N., and C. D. Keeling, Seasonal carbon cycling in the Sargasso Sea near Bermuda, *Bull. Scripps Inst. Oceanogr.*, in press, 1999.

Gruber, N., J. L. Sarmiento, and T. F. Stocker, An improved method for detecting anthropogenic CO_2 in the oceans, *Global Biogeochem. Cycles, 10*(4), 809–837, 1996.

Gruber, N., C. D. Keeling, and T. F. Stocker, Carbon-13 constraints on the seasonal inorganic carbon budget at the BATS site in the northwestern Sargasso Sea, *Deep Sea Res., Part I, 45*, 673–717, 1998.

Heimann, M., and E. Maier-Reimer, On the relations between the oceanic uptake of CO_2 and its carbon isotopes, *Global Biogeochem. Cycles, 10*(1), 89–110, 1996.

Joos, F., and M. Bruno, Long-term variability of the terrestrial and oceanic carbon sinks and the budgets of the carbon isotopes ^{13}C and ^{14}C, *Global Biogeochem. Cycles, 12*(2), 277–295, 1998.

Joyce, T. M., and P. Robbins, The long-term hydrographic record at Bermuda, *J. Clim., 9*(12), 3121–3131, 1996.

Karl, D. M., and R. Lukas, The Hawaii Ocean Time-series (HOT) program: Background, rationale and field implementation, *Deep Sea Res., Part II, 43*, 129–156, 1996.

Keeling, C. D., The Suess Effect: ^{13}Carbon and ^{14}Carbon interactions, in *Environment International*, vol. 2, pp. 229–300, Pergamon, Tarrytown, N.Y., 1979.

Keeling, C. D., NATO lecture 2: Surface ocean CO_2, in *The Global Carbon Cycle*, edited by M. Heimann, pp. 413–430, Springer-Verlag, New York, 1993.

Keeling, C. D., and R. Revelle, Effects of El Niño/Southern Oscillation on the atmospheirc content of carbon dioxide, *Meteoritics, 20*(2), 437–450, 1985.

Keeling, C. D., and T. P. Whorf, Possible forcing of global temperature by the oceanic tides, in *Carbon Dioxide and Climate Change*, edited by C. D. Keeling, pp. 8321–8328, Nat. Acad. of Sci., Washington, D. C., 1997.

Keeling, C. D., R. B. Bacastow, A. F. Carter, S. C. Piper, T. P. Whorf, M. Heimann, W. G. Mook, and H. Roeloffzen, A three dimensional model of atmospheric CO_2 transport based on observed winds, 1, Analysis of observational data, in *Aspects of Climate Variability in the Pacific and the Western Americas, Geophys. Monogr. Ser.*, vol. 55, edited by D. H. Peterson, pp. 165–237, AGU, Washington, D.C., 1989.

Keeling, C. D., T. P. Whorf, M. Wahlen, and J. v. d. Plicht, Interannual extremes in the rate of atmospheric carbon dioxide since 1980, *Nature, 375*, 666–670, 1995.

Keir, R. S., The effect of vertical nutrient redistribution on surface ocean ^{13}C, *Global Biogeochem. Cycles, 5*(4), 351–358, 1991.

Kroopnick, P., The distribution of ^{13}C in the Atlantic Ocean, *Earth Planet. Sci. Lett., 49*, 469–484, 1980.

Kroopnick, P. M., The distribution of ^{13}C of TCO_2 in the world oceans, *Deep Sea Res., 32*, 57–84, 1985.

Kroopnick, P. M., S. V. Margolis, and C. S. Wong, ^{13}C variations in marine carbonate sediments as indicators of the CO_2 balance beteen atmosphere and oceans, in *The Fate of Fossil Fuel CO_2 in the Oceans*, edited by N. Andersen and A. Malahoff, pp. 295–321, Plenum, New York, 1977.

Lueker, T. J., The ratio of the first and second dissociation constants of carbonic acid determined from the concentration of carbon dioxide in gas and seawater at equilibrium, Ph. D. thesis, Scripps Inst. of Oceanogr., Univ. of Calif., San Diego, 1998.

Lynch-Stieglitz, J., T. F. Stocker, W. S. Broecker, and R. G. Fairbanks, The influence of air-sea exchange on the isotopic composition of oceanic carbon: Observations and modeling, *Global Biogeochem. Cycles, 9*(4), 653–665, 1995.

Mehrbach, C., C. H. Culberson, J. E. Hawley, and R. M. Pytkowicz, Measurement of the apparent dissociation constants of carbonic acid in seawater at atmospheric pressure, *Limnol. Oceanogr., 18*, 897–907, 1973.

Michaels, A. F., and A. H. Knap, Overview of the U.S. JGOFS Bermuda Atlantic Time-series Study and the Hydrostation S program, *Deep Sea Res., Part II, 43*, 157–198, 1996.

Millero, F. J., Thermodynamics of the carbon dioxide system in the oceans, *Geochim. Cosmochim. Acta, 59*(4), 661–677, 1995.

Mook, W. G., ^{13}C in atmospheric CO_2, *Neth. J. Sea Res., 20*(2/3), 211–223, 1986.

Mook, W. G., and P. M. Grootes, The measuring procedure and corrections for the high-precision mass-spectrometric analysis of isotopic abundance ratios, especially referring to carbon, oxygen and nitrogen, *Int. J. Mass Spectrom. Phys., 12*, 273–298, 1973.

Mook, W. G., M. Koopmans, A. F. Carter, and C. D. Keeling, Seasonal, latitudinal and secular variations in the abundance and isotopic ratios of atmospheric carbon dioxide, 1, Results from land stations, *J. Geophys. Res., 88*(C15), 10915–10933, 1983.

O'Leary, M. H., Carbon isotope fractionation in plants, *Phytochem., 20*, 553–567, 1981.

Peng, T.-H., and W. S. Broecker, C/P ratios in marine detritus, *Global Biogeochem. Cycles, 1*(2), 155–161, 1987.

Quay, P. D., B. Tilbrook, and C. S. Wong, Oceanic uptake of fossil fuel CO_2: Carbon-13 evidence, *Science, 256*, 74–79, 1992.

Rau, G. H., T. Takahashi, and D. J. D. Marais, Latitudinal variations in plankton $\delta^{13}C$: Implications for CO_2 and productivity in past oceans, *Nature, 341*, 516–518, 1989.

Roeloffzen, J. C., The calibration of ^{13}C and ^{18}O measurements, 1977-1991, in *Centre for Isotope Physics, Tech. Rep.*, Groningen, Netherlands, 1993.

Sabine, C. L., R. M. Key, K. M. Johnson, F. J. Millero, J. L. Sarmiento, D. W. R. Wallace, and C. D. Winn, Anthropogenic CO_2 inventory of the Indian Ocean, *Global Biogeochem. Cycles*, *13*(1), 179–198, 1999.

Sarmiento, J. L., J. C. Orr, and U. Siegenthaler, A perturbation simulation of CO_2 uptake in an ocean general circulation model, *J. Geophys. Res.*, *97*(C3), 3621–3645, 1992.

Siegenthaler, U., and K. O. Münnich, $^{13}c/^{12}c$ fractionation during CO_2 transfer from air to sea, in *SCOPE 16: Carbon Cycle Modelling*, edited by B. Bolin, pp. 249–257, John Wiley, New York, 1981.

Spero, H. J., J. Bijma, D. W. Lea, and B. E. Bemis, Effect of seawater carbonate concentration on foraminiferal carbon and oxygen isotopes, *Nature*, *390*, 497–500, 1997.

Takahashi, T., W. Broecker, S. Werner, and A. E. Bainbridge, Carbonate chemistry of the surface waters of the world oceans, in *Isotope Marine Chemistry*, edited by E. D. Goldberg, Y. Horibe, and K. Saruhashi, pp. 291–326, Uchida Rokakuho, Tokyo, 1980.

Takahashi, T., W. S. Broecker, and A. E. Bainbridge, The alkalinity and total carbon dioxide concentration in the world oceans, in *Scope 16: Carbon Cycle Modelling*, edited by B. Bolin, pp. 271–286, John Wiley, New York, 1981.

Takahashi, T., W. S. Broecker, and S. Langer, Redfield ratio based on chemical data from isopycnal surfaces, *J. Geophys. Res.*, *90*(C4), 6907–6924, 1985.

Tans, P., A compilation of bomb ^{14}C data for use in global carbon model calculation, in *SCOPE 16: Carbon Cycle Modelling*, edited by B. Bolin, pp. 131–137, John Wiley, New York, 1981.

Tans, P. P., J. A. Berry, and R. F. Keeling, Oceanic $^{12}C/^{13}C$ observations: A new window on ocean CO_2 uptake, *Global Biogeochem. Cycles*, *7*(2), 353–368, 1993.

Trenberth, K. E., and T. J. Hoar, The 1990-1995 El Niño-Southern Oscillation event: Longest on record, *Geophys. Res. Lett.*, *23*(1), 57–60, 1996.

Trenberth, K. E., and T. J. Hoar, El Niño and climate change, *Geophys. Res. Lett.*, *24*(23), 3057–3060, 1997.

UNESCO, Background papers and supporting data on the practical salinity scale, in *UNESCO technical papers in marine science, 37*, Paris, 1981.

Wallace, D. W. R., Monitoring global ocean carbon inventories, *OOSDP Background Report, 5*, Ocean Obs. Syst. Dev. Panel, Texas A&M Univ., College Station, 1995.

Whitworth, T., III, and W. D. Nowlin Jr., Water masses and currents of the Southern Ocean at the Greenwich Meridian, *J. Geophys. Res.*, *92*(C6), 6462–6476, 1987.

Zhang, J., P. D. Quay, and D. O. Wilbur, Carbon isotope fractionation during gas-water exchange and dissolution of CO_2, *Geochim. Cosmochim. Acta*, *59*(1), 107–114, 1995.

N. Gruber, Atmospheric and Oceanic Sciences Program, Princeton University, Sayre Hall, Forrestal Campus, P.O. Box CN710, Princeton, NJ 08544-0710. (gruber@splash.princeton.edu)

R. B. Bacastow, P. R. Guenther, C. D. Keeling, T.J. Lueker, and M. Wahlen, Scripps Institution of Oceanography, University of California, San Diego, La Jolla, CA 92093-0220. (rbacastow@ucsd.edu; pguenther@ucsd.edu; cdkeeling@ucsd.edu; tlueker@ucsd.edu; mwahlen@ucsd.edu)

H. A. J. Meijer and W. G. Mook, Centrum voor Isotopen Onderzoek, University of Groningen, 9722 JX Groningen, Netherlands. (meijer@phys.rug.nl)

T. F. Stocker, Climate and Environmental Physics, Physics Institute, University of Bern, Sidlerstr. 5, 3012 Bern, Switzerland. (stocker@climate.unibe.ch)

(Received August 11, 1998; revised February 24, 1999; accepted February 26, 1999.)